Molecular Therapy
Original Article

Targeting circular RNA-MET for anti-angiogenesis treatment via inhibiting endothelial tip cell specialization

Mu-Di Yao,[1,2,3,6] Qin Jiang,[4,5,6] Yan Ma,[5,6] Yan Zhu,[5,6] Qiu-Yang Zhang,[4,5,6] Ze-Hui Shi,[1,2] Chen Zhao,[1] and Biao Yan[1,2,3]

[1]Eye Institute, Eye & ENT Hospital, Shanghai Medical College, Fudan University, Shanghai, China; [2]NHC Key Laboratory of Myopia (Fudan University), Key Laboratory of Myopia, Chinese Academy of Medical Sciences, Shanghai, China; [3]Shanghai Key Laboratory of Visual Impairment and Restoration (Fudan University), Shanghai, China; [4]The Affiliated Eye Hospital, Nanjing Medical University, Nanjing, China; [5]The Fourth School of Clinical Medicine, Nanjing Medical University, Nanjing, China

Endothelial tip cell specialization plays an essential role in angiogenesis, which is tightly regulated by the complicated gene regulatory network. Circular RNA (circRNA) is a type of covalently closed non-coding RNA that regulates gene expression in eukaryotes. Here, we report that the levels of circMET expression are significantly upregulated in the retinas of mice with oxygen-induced retinopathy, choroidal neovascularization, and diabetic retinopathy. circMET silencing significantly reduces pathological angiogenesis and inhibits tip cell specialization *in vivo*. circMET silencing also decreases endothelial migration and sprouting *in vitro*. Mechanistically, circMET regulates endothelial sprouting and pathological angiogenesis by acting as a scaffold to enhance the interaction between IGF2BP2 and NRARP/ESM1. Clinically, circMET is significantly upregulated in the clinical samples of the patients of diabetic retinopathy. circMET silencing could reduce diabetic vitreous-induced endothelial sprouting and retinal angiogenesis *in vivo*. Collectively, these data identify a circRNA-mediated mechanism that coordinates tip cell specialization and pathological angiogenesis. circMET silencing is an exploitable therapeutic approach for the treatment of neovascular diseases.

INTRODUCTION

Well-regulated angiogenesis plays important roles in many physiological processes, including embryonic development, organ growth, and tissue repair. Abnormal angiogenesis is the pathological basis of many human disorders, such as malignant, inflammatory, ischemic, and immune disorders.[1,2] Angiogenesis is a critical, fine-tuned, and multi-staged process, which involves the complicated interactions between endothelial cells (ECs) and other vascular cells.[3,4] ECs are highly heterogeneous in terms of the functional properties and gene expression profiles. In response to the pro-angiogenic signals, a fraction of ECs acquire tip cell phenotype, which can extend filopodia to probe environmental cues and mediate vascular elongation.[5] ECs behind tip cells acquire stalk cell phenotype, which usually generate fewer filopodia and proliferate to mediate sprout elongation and vascular lumen formation.[6] Endothelial tip cell specialization is a key event of angiogenesis, which is tightly associated with the extension of vascular networks.

Endothelial tip cell specialization has been characterized in mouse retina, endothelial spheroid, and retinal angiogenesis/choriocapillaris sprouting model in zebrafish.[7,8] The retina is a unique site where the vasculature can be observed directly. The easily accessible vasculature provides an opportunity to study the mechanism of tip cell specialization.[9,10] Pathological angiogenesis has been observed in several vision-threatening diseases, such as retinopathy of prematurity, diabetic retinopathy, and age-related macular degeneration. Vascular endothelial growth factor (VEGF) has been found to be a key driver of pathological angiogenesis. However, some patients have poor or no response to current anti-VEGF treatments and usually have some side effects, such as rare infectious, noninfectious endophthalmitis, retinal detachment, and increased intraocular pressure.[11–13] Clarifying the mechanism of tip cell specialization contributes to the identification of novel targets for the treatment of neovascular diseases.

The precise mechanism that regulates tip cell speciation is still subject to debate. Notch-VEGFR pathway, Slit-Robo pathway, Semaphorin pathway, and ECM-integrin pathway are potentially involved in the regulation of tip cell specification.[4] However, these pathways always interfere with each other. Recent studies have revealed that epigenetic modifications have great impacts on the process of angiogenesis. Non-coding RNAs (ncRNAs) play important roles in angiogenic-associated networks through the transcriptional or post-transcriptional regulation of gene expression.[14,15] Among the distinct ncRNA types, circular RNAs (circRNAs) are a class of covalently closed, endogenous

Received 29 October 2021; accepted 5 January 2022;
https://doi.org/10.1016/j.ymthe.2022.01.012.

[6]These authors contributed equally

Correspondence: Biao Yan, Fudan University, 83# Fen Yang Road, Shanghai 200030, China.
E-mail: biao.yan@fdeent.org

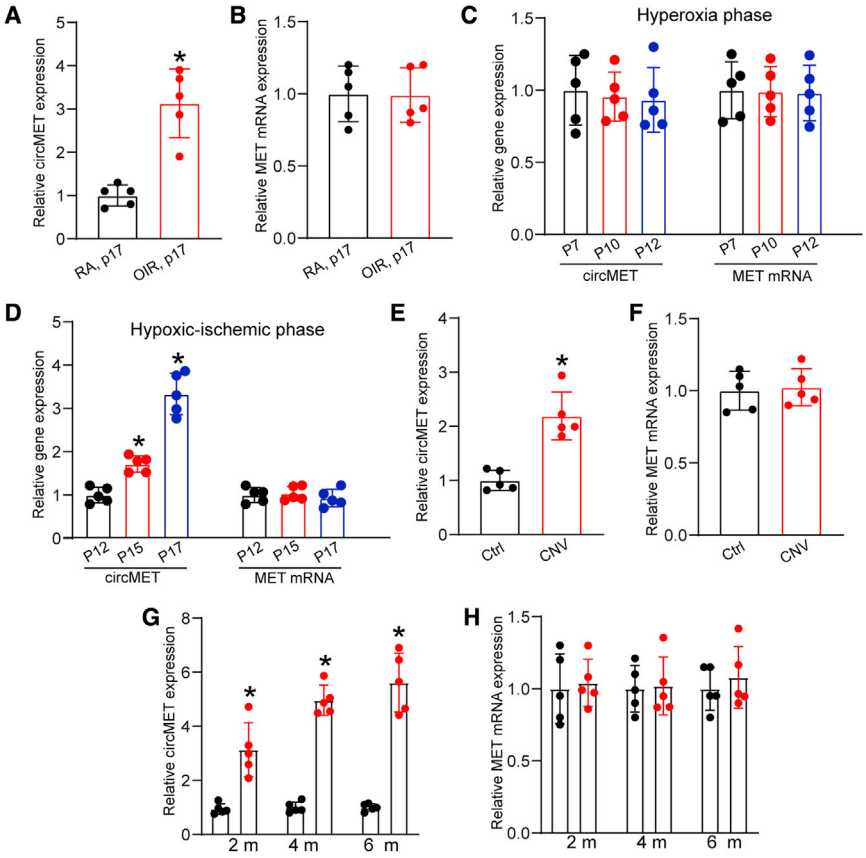

Figure 1. circMET is significantly upregulated in pathological angiogenesis

(A and B) The neonatal mice with their nursing mothers were exposed to 75% O_2 from postnatal day (P) 7 to P12 and then returned to room air until P17. qRT-PCR assays were conducted to detect the expression levels of circMET and MET mRNA at P17 (n = 5 mice per group). (C and D) The retinas were obtained from the mice at the indicated time points. qRT-PCR assays were conducted to detect the levels of circMET and MET mRNA. Data were normalized to both the expression of internal control and to gene expression at P7 or P12 (n = 5 mice per group). (E and F) qRT-PCRs were conducted to detect the expression levels of circMET and MET mRNA in the choroid tissues of C57BL/6J mice at 2 weeks after laser injury (n = 5 mice per group). (G and H) The expression levels of circMET and MET mRNA were detected by qRT-PCRs in the retinal vessels isolated from the nondiabetic retinas and diabetic retinas at 2 months, 4 months, and 6 months after diabetes induction (n = 5 mice per group). Mann-Whitney *U* test (A, B, E, F, G, and H); Kruskal-Wallis's test followed by Bonferroni's post hoc test (C and D); *p < 0.05.

non-coding RNAs without 5′ end caps or 3′ poly(A) tails.[16] They are expressed in tissue-specific, cell-specific, and developmental stage-specific patterns.[17] circRNAs can regulate gene expression by acting as microRNA (miRNA) sponges, protein sponges, decoys, scaffolds, and recruiters. The high abundance, stability, and evolutionary conservation among different species endow circRNAs with many biological functions.[18] Aberrant circRNA expression has been observed in several human disorders, including cancers, neurological diseases, and cardiovascular diseases.[19] However, the role of circRNAs in endothelial tip specialization remains unclear.

In this study, we mainly investigate the role of hsa_circ_0082002 in endothelial tip cell specialization. As reported in circBase database, this circular RNA is located at chr7: 116,339,124–116,340,338 in human genome and highly expressed in endothelial cells. Moreover, it is highly conserved between human genome and mouse genome (mmu_circ_0013214). Our result shows that circMET is significantly upregulated in pathological angiogenesis. circMET silencing suppresses retinal and choroidal angiogenesis by inhibiting endothelial tip cell specialization. circMET regulates endothelial migration and sprouting via circMET/IGF2BP2/NRARP or ESM1 complex. Clinically, circMET is significantly upregulated in the clinical samples of DR patients. This study indicates that circMET is a promising predictor or a therapeutic target for neovascular diseases.

RESULTS

circMET is significantly upregulated in pathological angiogenesis

To determine the role of circMET in pathological angiogenesis, we first detected the expression pattern of circMET in the retinas of mouse model of oxygen-induced retinopathy (OIR). qRT-PCR assays showed that the levels of circMET were significantly upregulated, whereas the levels of MET mRNA did not alter on the postnatal day (P)17 in OIR retinas, compared with the controls in room air (Figures 1A and 1B). We next performed a time course analysis of circMET and MET mRNA expression from P7 to P12 (hyperoxia phase) and from P12 to P17 (hypoxic-ischemic phase) in OIR retinas. We did not observe the expression change of MET mRNA or circMET from P7 to P12 (Figure 1C), whereas the expression of circMET steadily increased from P12 to P17 (Figure 1D), showing a sustained increase in circMET expression throughout the hypoxic-ischemic phase.

Laser-induced choroidal neovascularization (CNV) murine model is another model for studying ocular angiogenesis.[20] Adult C57BL/6 mice were subjected to the rupture of Bruch's membrane by laser photocoagulation. qRT-PCR assays showed that the levels of circMET were significantly upregulated in the choroidal tissues at 2 weeks after laser injury, while the level of MET mRNA did not alter (Figures 1E and 1F). Streptozotocin (STZ) was administered to 8-week-old C57BL/6J mice over 5 consecutive days to build a diabetic murine model. Retinal vessels were extracted from the retinas at 2 months, 4 months, and 6 months after the induction of diabetes. The expression levels of circMET but not MET mRNA were significantly upregulated in diabetic vessels compared with the nondiabetic controls

(Figures 1G and 1H). Human retinal vascular endothelial cells (HRVECs) were also exposed to hypoxia (1% O_2) for 12 h or 24 h to mimic hypoxic condition during angiogenesis *in vitro*. qRT-PCR assays showed that the levels of circMET but not MET mRNAs were significantly upregulated in the hypoxic group compared with the normoxic control group (Figures S1A and S1B). HIF-1α is an important transcriptional regulator in hypoxic response. Hypoxia-induced circMET upregulation was abrogated upon HIF-1α silencing in hypoxic condition (Figure S1C).

circMET regulates pathological angiogenesis and tip cell specialization *in vivo*

Given the induction of circMET in pathological angiogenesis, we postulated that circMET was involved in maintaining vascular stability. We designed Cre-dependent circMET shRNA and injected it into the vitreous body of Cdh5-Cre mice. Intravitreous injection of Cre-dependent circMET shRNA in Cdh5-Cre mice led to decreased circMET expression in endothelial cells but not in pericytes (Figure S2A).

We first used the OIR model to investigate the role of circMET in retinal angiogenesis. The results showed that circMET silencing in OIR model led to decreased avascular area, reduced angiogenesis, and decreased vascular tufts compared with that in the control mice at P17 (Figure 2A). In the angiogenic area, circMET silencing led to a decreased number of vascular tip cells and filopodia (Figure 2B). We further adopted a laser-induced CNV model to determine the role of circMET in choroidal neovascularization. The eyes were collected on day 14 after laser injury. As shown in Figure S2B, >85% knockdown efficiency of choroidal tissue was achieved by subretinal injection of circMET shRNA compared with the controls. IB-4 staining showed that circMET silencing repressed CNV area by >50% compared with the controls (Figure 2C). On day 3, day 7, and day 14 after laser photocoagulation, CNV lesions were stained with IB-4 and VEGFR2 to label CNV area and endothelial tip cells. The result showed that circMET silencing significantly reduced CNV area and decreased the number of tip cells (Figure 2D).

circMET regulates endothelial tip specialization *in vitro* and *ex vivo*

Angiogenesis is largely driven by endothelial tip cells, which can invade avascular tissues and contribute to the formation of new vessels.[21] In HRVECs, transfection of circMET siRNA led to reduced expression of circMET but did not alter the expression of MET mRNA (Figure S3). To examine whether circMET regulated the formation of endothelial tip cells *in vitro*, we measured the expression of their signature genes. In HRVECs, circMET silencing led to reduced expression of tip cell-enriched genes (CXCR4, CD34, and VEGFA) and increased expression of stalk cell-enriched genes (HEY1, HEY2, and DLL4) under baseline condition (Figure 3A).

To examine the role of circMET in endothelial sprouting *in vitro*, we employed the spheroid sprouting assay and measure the sprouting length of endothelial spheroids. Compared with the control group, circMET silencing significantly reduced the sprouting length of endothelial spheroids (Figure 3B). We further examined whether circMET silencing affected the migration of endothelial cells *in vitro*. Transwell assays showed that compared with the control group, circMET silencing significantly reduced the migration ability of endothelial cells (Figure 3C). We also established an *ex vivo* choroidal sprouting explant model and examined the role of circMET in sprouting angiogenesis. The choroidal tissues from C57BL/6J mice were isolated and incubated in Matrigel. Compared with scramble shRNA-transfected explants or untreated explants, circMET silencing decreased the sprouting area and reduced choroidal sprouting on day 7 (Figure 3D).

We also showed that transfection of circMET overexpression vector led to increased levels of circMET expression in HRVECs and choroidal explants (Figure S4). circMET overexpression also led to increased expression of tip cell-enriched genes (CXCR4, CD34, and VEGFA), decreased expression of stalk cell-enriched genes (HEY1, HEY2, and DLL4), enhanced sprouting ability of endothelial spheroid, and increased migration ability of endothelial cells (Figure S5).

circMET interacts with IGF2BP in endothelial cells

Ago2 is the core component of miRNA-induced silencing (RISC) complex. miRNAs are generally associated with RISC complex that plays an important role in the regulation of gene expression.[22] If circMET plays its role by acting as the miRNA sponge in endothelial cells, circMET should be tightly associated with Ago2. We conducted RIP assays using Ago2 antibody to detect the interaction between Ago2 and circMET. The results showed that circZNF609 (a circRNA binding with Ago2)[23] but not circMET was significantly enriched by Ago2 antibody, suggesting that circMET may not act as a miRNA sponge in HRVECs (Figure S6A).

To determine whether circMET exerted its function via interacting with proteins, we predicted circMET-interacting proteins by circAtlas 2.0 database and Circular RNA Interactome database. IGF2BPs were predicted to be potentially interacted with circMET. Moreover, IGF2BPs played an important role in post-transcriptional control of gene expression. qRT-PCR assays showed that the sense probe for circMET could efficiently and specifically enrich circMET but not MET mRNA (Figures S6B and S6C).

RNA pull-down and RIP analysis confirmed the interaction between IGF2BPs and circMET. Notably, IGF2BP2 could pull down a greater amount of circMET than IGF2BP1 or IGF2BP3 (Figures 4A and 4B). RNA-FISH and immunofluorescence analysis showed that circMET co-localized with IGF2BPs in the cytoplasm of HRVECs. The merged area between circMET and IGF2BP2 was significantly greater than the merged area of circMET/IGF2BP1 or circMET/IGF2BP3 (Figure 4C). Given there were some non-specific interactions between circMET and IGF2BP1/3 (Figure 4A), we subsequently focused on circMET-IGF2BP2 interaction in the following study.

m^6A modification is mainly mediated by methyltransferase-like 3 (METTL3) and methyltransferase-like 14 (METTL14) heterodimer.[24]

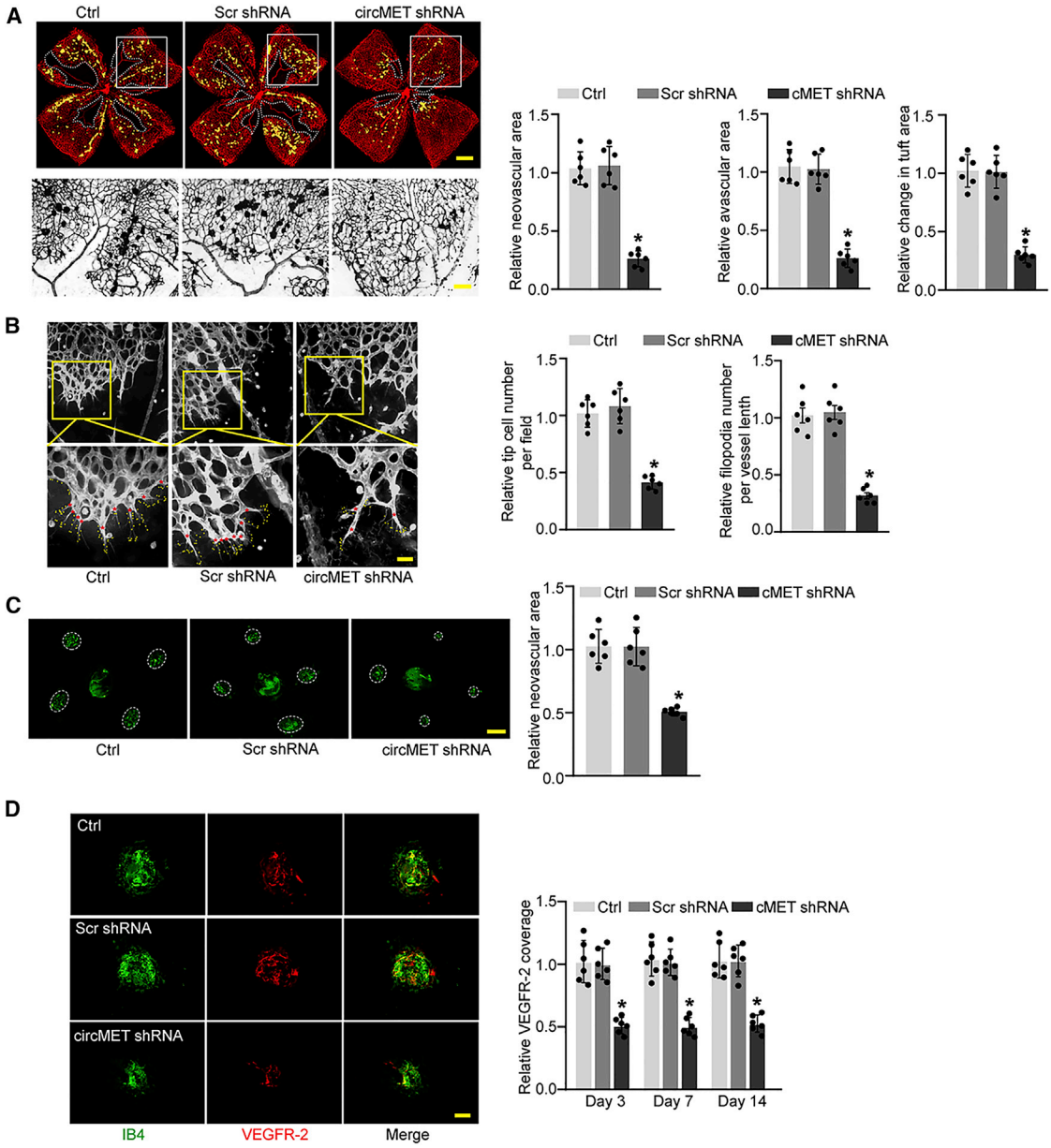

Figure 2. circMET silencing suppresses pathological angiogenesis and tip cell specialization *in vivo*

(A and B) The neonatal mouse received an injection of scrambled (Scr) shRNA, Cre-dependent circMET shRNA, or left untreated (Ctrl). On the postnatal day 7 (P7), the mouse pups with their nursing mothers were subjected to hyperoxia (75% O_2) for 5 days, and then returned to room air on P12. The retinas were harvested on P17 and stained with Isolectin B4 (IB4) to show retinal vasculature. Yellow staining indicated neovascular area; Low panels showed high magnification of neovascular tufts. Scale bars: upper panel, 1 mm; lower panels, 100 μm. The quantification results of neovascular area, avascular area, and neovascular tufts were shown (A, n = 6 mice per group). (B) At the angiogenic front, the quantification results of filopodia (yellow dots) and tip cells (red asterisk) were shown. Scale bar: 50 μm (B, n = 6 mice per group). (C and D) RPE/choroid complexes were dissected and flat-mounted on day 14 after laser photocoagulation. The blood vessels were stained with IB-4 and neovascular area was calculated. The representative images of IB-4 staining are shown. Green staining indicates CNV lesion. Dashed line indicates CNV area. Scale bar: 200 μm (C, n = 6 mice per group). On day 3, day 7, and day 14 after laser photocoagulation, CNV lesions were stained with IB-4 and VEGFR2 to label choroidal neovascularization and vascular tip cells. Scale bar: 50 μm (D, n = 6 mice per group). All significant difference was determined by Kruskal-Wallis's test followed by Bonferroni's post hoc test; *$p < 0.05$.

To explore whether the circMET-IGF2BP2 interaction was regulated via the m^{6}A-dependent manner, we conducted m^{6}A RNA immunoprecipitation (MeRIP) of circMET and observed a significant enrichment of circMET in m^{6}A immunoprecipitate. By contrast, knockdown of METTL3 and METTL14 decreased the level of circMET in m^{6}A immunoprecipitate (Figure 4D). We also found that knockdown

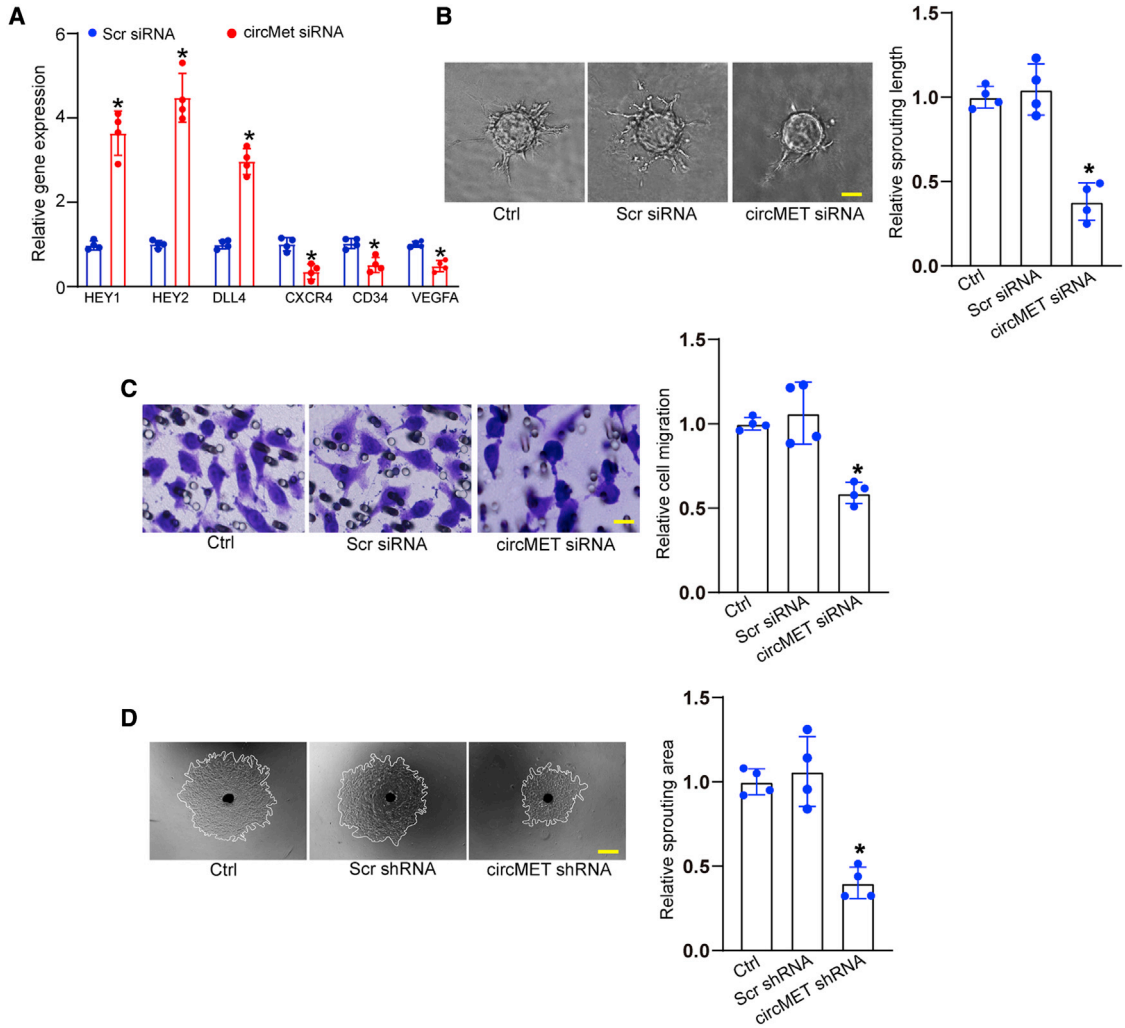

Figure 3. circMET regulates endothelial tip cell specialization *in vitro* and *ex vivo*

(A) HRVECs were transfected with scramble (Scr) siRNA or circMET siRNA for 24 h. qRT-PCR assays were conducted to detect the expression of CXCR4, CD34, VEGFA, HEY1, HEY2, and DLL4. n = 4; Student's t test, *p < 0.05 versus Scr group. (B) HRVECs were transfected with Scr siRNA, circMET siRNA, or left untreated (Ctrl) for 24 h. *In vitro* spheroid sprouting assay and quantitative analysis was conducted to detect the role of circMET in endothelial sprouting. Scale bar: 100 μm. n = 4; one-way ANOVA followed by Bonferroni's post hoc test, *p < 0.05 versus Ctrl group. (C) Transwell assay and quantitative analysis conducted to detect the role of circMET in endothelial migration. Scale bar: 50 μm. n = 4; one-way ANOVA followed by Bonferroni's post hoc test, *p < 0.05 versus Ctrl group. (D) Cdh5-Cre mice received a subretinal injection of Scr shRNA, Cre-dependent circMET shRNA, or left untreated (Ctrl). On day 14, RPE/choroid complexes were dissected. The peripheral regions of RPE complexes were cut into 1 mm × 1 mm pieces and seeded. The sprouting ability of choroidal explants were photographed on day 7. The representative images and quantification results of choroidal sprouting are shown. n = 4; Scale bar: 500 μm. *p < 0.05 versus Ctrl group; one-way ANOVA followed by Bonferroni's post hoc test.

of METTL3 or METTL14 did not alter the level of circMET (Figures 4E and 4F). IGF2BP2 preferentially bound to the "(U > C) GGAC" consensus,[25] and we identified two potential IGF2BP2-binding regions (CGGACC) in circMET sequence. circMET mutant was constructed with the mutation from "CGGACC" to "GCCUGG." circMET-IGF2BP2 interaction was remarkably impaired in METTL3/14 knockdown group or circMET mutant group (Figure 4G). These data reveal that circMET physically interacts with IGF2BP2 in an m^{6}A-dependent manner.

Since IGF2BP2 could interact with m^{6}A-modified RNAs, we further determined whether altered IGF2BP2 level affected the stability of circMET. RNA stability assay showed that the level of circMET in the IGF2BP2 overexpression group was slightly higher than that in the control group (Figure S7A). Moreover, MeRIP-PCR assay showed that IGF2BP2 overexpression significantly increased the level of m^{6}A-modified circMET in HRVECs (Figure S7B), suggesting that IGF2BP2 plays an important in the regulation of circMET stability.

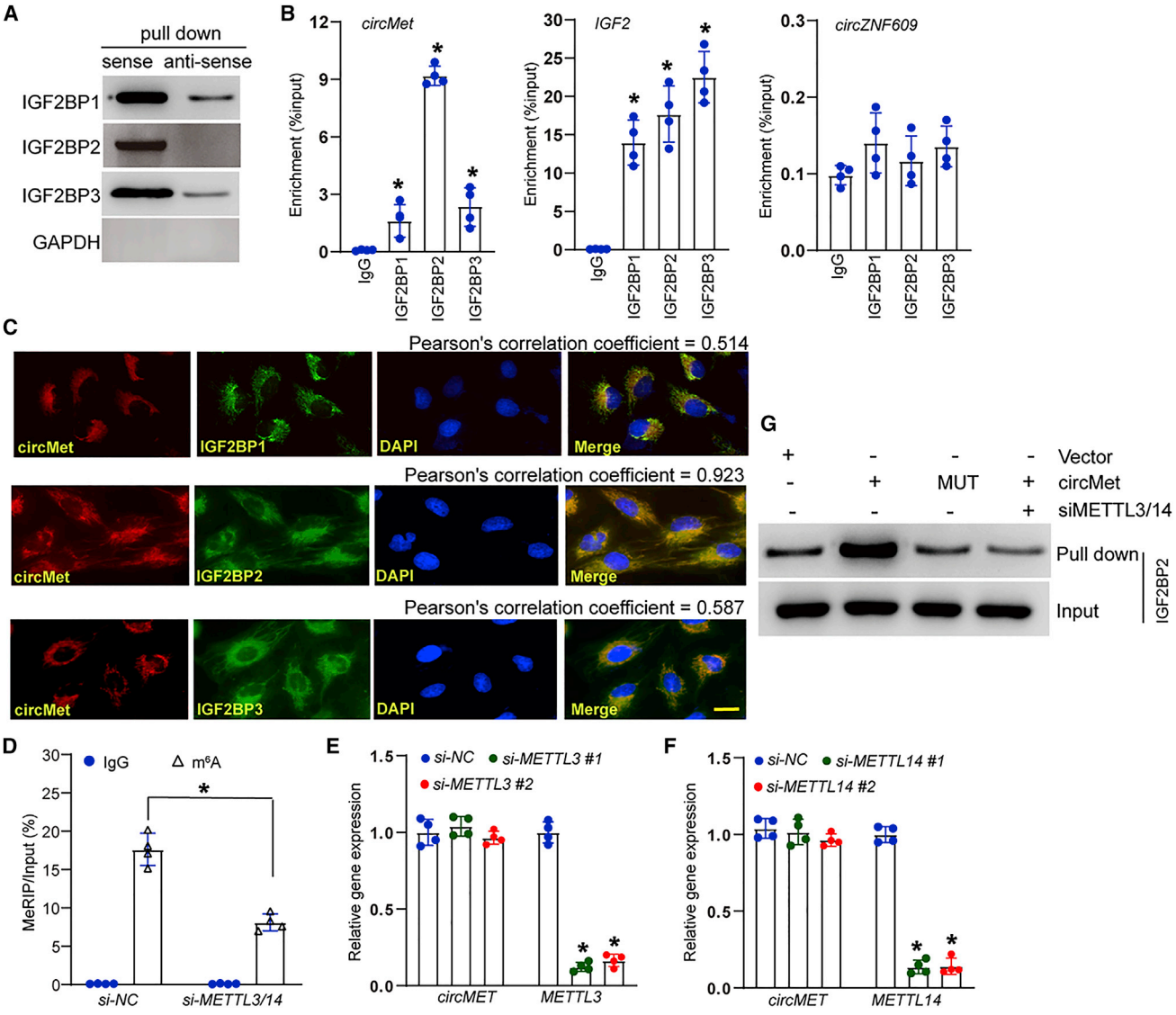

Figure 4. circMET interacts with IGF2BP in endothelial cells

(A) RNA pull-down assays were conducted to detect the interaction between IGF2BPs and circMET using the biotinylated sense- or anti-sense probe targeting circMET back-splice junction region. (B) RIP assay was conducted using IgG and IGF2BPs to detect the enrichment of circMET, IGF2 (a positive control), and circZNF609 (a negative control). n = 4; *p < 0.05 versus IgG group, one-way ANOVA followed by Bonferroni's post hoc test. (C) RNA-FISH and immunofluorescence was conducted to detect the co-localization of circMET (red) with IGF2BP proteins (green) in HRVECs. Scale bar: 50 μm. (D) Gene-specific m^{6}A qRT-PCR assays were conducted to detect m^{6}A modification of circMET in HRVECs with or without METTL3/14 knockdown. n = 4; *p < 0.05 m^{6}A in negative siRNA (si-*NC*) group versus m^{6}A in si-*METTL3/14* group, Student's t test. (E) Expression levels of METTL3 and circMET in HRVECs with METTL3 knockdown. n = 4; *p < 0.05 versus si-*NC* group, one-way ANOVA followed by Bonferroni's post hoc test. (F) Expression levels of METTL14 and circMET in HRVECs cells with METTL14 knockdown. n = 4; *p < 0.05 versus si-*NC* group, one-way ANOVA followed by Bonferroni's post hoc test. (G) RNA pull-down assays were conducted to detect the interaction between circMET and IGF2BP2 in the indicated group (MUT: mutated circMET without m^{6}A motif).

circMET plays its role via the formation of circMET/IGF2BP2/NRARP or ESM1 complex

As IGF2BP2 is essential for mRNA stability,[26] we then wondered if the circMET/IGF2BP2 complex stabilized certain unknown downstream targets. We conducted RNA-SEQ analysis in HRVECs. 942 mRNAs showed a significant decrease in mRNA expression upon circMET silencing (Table S1; fold change >3, $P < 0.01$). Previous study has revealed that IGF2BP2 preferentially binds to 3′-UTR of target mRNAs with high AU content.[25] Among the downregulated mRNAs, we screened IGF2BP2-binding 3′-UTRs from the published RBP CLIP-SEQ datasets. Given that the role of circMET in angiogenesis, we focused on these angiogenesis-related genes as the potential targets

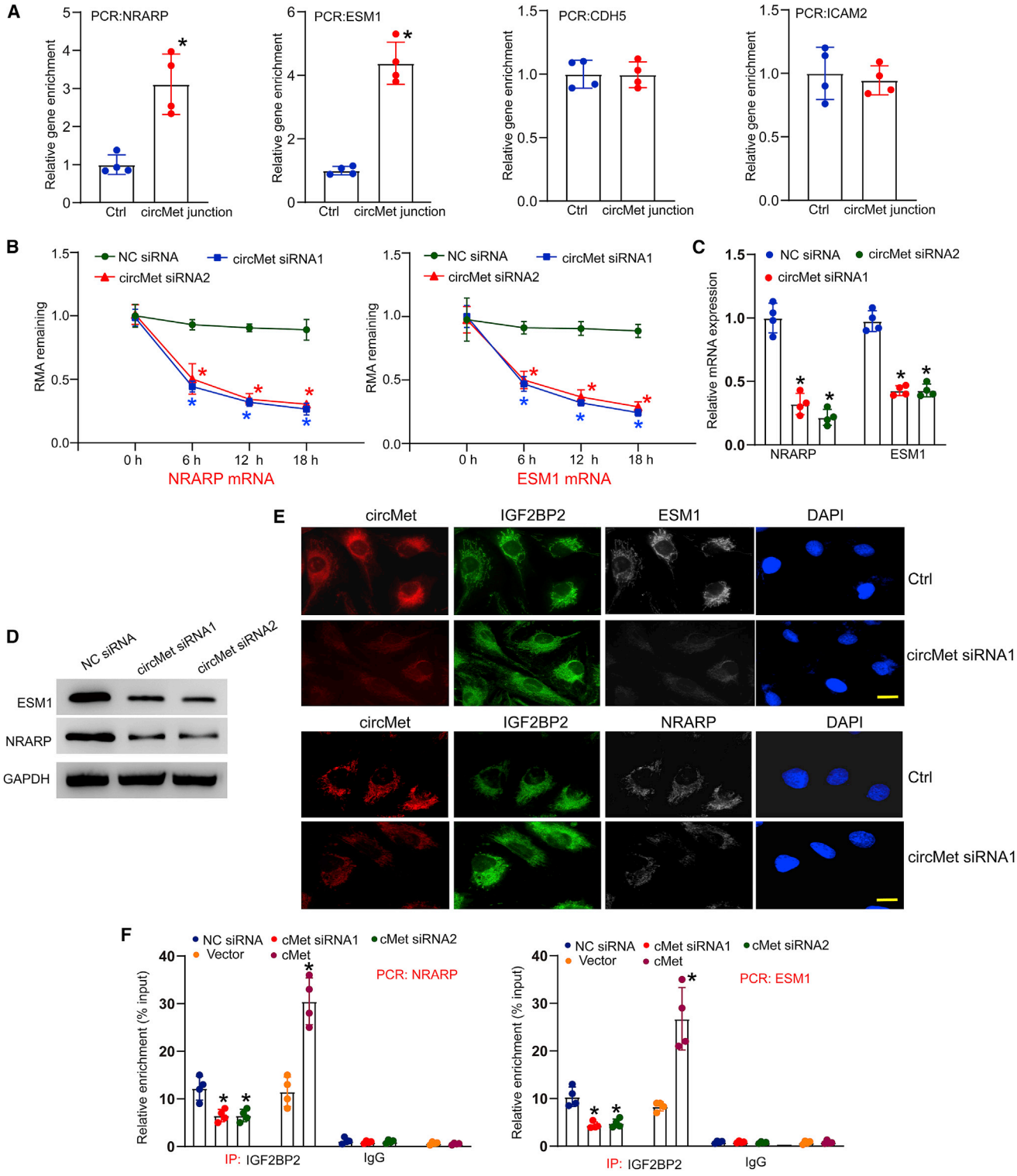

Figure 5. circMET plays its role via the formation of circMET/IGF2BP2/NRARP or ESM1 complex

(A) RNA pull-down assays were conducted using the biotinylated sense or anti-sense probe (Ctrl), which targets the circMET back-splice junction region. PCR assays were conducted to detect the relative enrichment of NRARP, ESM1, CDH5, and ICAM2. n = 4; Student's t test. (B) HRVECs were transfected with negative siRNA (si-NC), circMET siRNA1, or circMET siRNA2. The remaining amount of NRARP and ESM1 was determined by qRT-PCR assay. n = 4; two-way ANOVA followed by the Bonferroni post hoc

(legend continued on next page)

of circMET, including NRARP, CDH5, ESM1, and ICAM2. RNA pull-down assays revealed the direct interaction between circMET and NRARP or ESM1 (Figure 5A). circMET silencing decreased the stability of NRARP or ESM1 mRNA (Figure 5B), which consequently led to reduced expression of NRARP or ESM1 at mRNA level and protein level (Figures 5C and 5D). By contrast, enforced expression of circMET led to increased expression of NRARP and ESM1 (Figure S8).

We further verified that circMET/IGF2BP2/NRARP or ESM1 formed an RNA-protein complex, which was supported by the following evidence. RNA-FISH and immunofluorescence assays showed that NRARP/ESM1 and IGF2BP2 were co-localized in the cytoplasm. In the absence of circMET, the co-localization of NRARP/IGF2BP2 or ESM1/IGF2BP2 complex was significantly decreased (Figure 5E), while IGF2BP2 expression did not alter. RIP assays showed that the amount of NRARP or ESM1 precipitated by IGF2BP2 was significantly greater than the amount of NRARP or ESM1 precipitated by IgG. circMET silencing significantly reduced the interaction of NRARP/IGF2BP2 or ESM1/IGF2BP2. By contrast, circMET overexpression significantly increased the enrichment of NRARP or ESM1 in IGF2BP2 immunoprecipitated fraction (Figure 5F). We further performed immunoprecipitation assays to determine whether circMET/IGF2BP2/NRARP or ESM1 formed a complex. After immunoprecipitation by IGF2BP2 or IgG, western blot analysis revealed that NRARP or ESM1 could be immunoprecipitated by IGF2BP2 in wild-type HRVECs but not in HRVECs without circMET expression (Figure S9). Collectively, these findings demonstrate that circMET plays a critical role in promoting the interaction between IGF2BP2 and NRARP/ESM1, and it enhances the mRNA stability of IGF2BP2 and NRARP/ESM1 through the formation of circMET/IGF2BP2/NRARP or ESM1 complex.

circMET regulates endothelial sprouting and pathological angiogenesis through NRARP/ESM1 pathway

We investigated whether circMET-mediated endothelial sprouting was dependent on NRARP/ESM1 pathway *in vitro*. Spheroid sprouting assays revealed that enforced expression of NRARP or ESM1 could functionally rescue circMET silencing-induced reduction of endothelial sprouting ability (Figure 6A). Transwell assays revealed that enforced expression of NRARP or ESM1 could reverse the reduction of migration ability caused by circMET silencing (Figure 6B). We further used a laser-induced CNV mouse model to determine whether circMET regulated pathological angiogenesis through NRARP/ESM1 pathway *in vivo*. circMET silencing significantly repressed the CNV area by >50% compared with the controls. Enforced expression of NRARP or ESM1 functionally rescued circMET silencing-induced CNV reduction in the CNV model (Figure 6C). On day 14 after laser photocoagulation, circMET silencing-induced reduction of vascular tip cells was largely restored by the overexpression of NRARP or ESM1 (Figure 6D).

Clinical implication of circMET/NRARP or ESM1 signaling in ocular vascular dysfunction

To further reveal the clinical relevance of circMET-mediated signaling in ocular vascular dysfunction, we determined the levels of circMET expression in a cohort of patients, including the patients with macular holes, patients with diabetic macular edema (DME) only, and patients with DME and proliferative diabetic retinopathy (PDR). qRT-PCRs showed that the levels of circMET expression were significantly upregulated in the vitreous samples of the patients with DME or DME+PDR. Notably, the levels of circMET expression were tightly correlated with the severity of retinal vascular dysfunction (Figure 7A). A second cohort of patients, anti-VEGF cohort, was used to determine the effects of anti-VEGF treatment on circMET expression. The levels of circMET expression were significantly downregulated in the vitreous samples of PDR patients who had received preoperative anti-VEGF therapy compared with that in the untreated PDR patients (Figure 7B). A third cohort of patients, non-PDR controls and PDR patients, were used to investigate the expression correlation between circMET and NRARP/ESM1. The results showed that the levels of NRARP or ESM1 expression were positively correlated with the levels of circMET expression (Figures 7C and 7D).

HRVECs were incubated with the vitreous from PDR patients. *In vitro* spheroid sprouting assay showed that stimulation with the vitreous from PDR patients dramatically increased the length and the number of vascular sprouting. By contrast, circMET silencing led to reduced vascular sprouting (Figure 7E). The mice received an intravitreal injection of PBS, diabetic vitreous without or with circMET shRNA. The result showed that injection of diabetic vitreous led to increased retinal vasopermeability and increased neovascular tuft area in mouse retinas. By contrast, circMET silencing significantly reduced diabetic vitreous-induced vascular leak and decreased the number of neovascular tufts (Figures 7F and 7G).

DISCUSSION

Angiogenesis is important for embryonic development and contributes to the onset and development of many human diseases.[27] Tip cell specialization is a critical step for angiogenesis.[10,28] Here, we show that circMET expression is significantly increased in the retinas of the mice with OIR, choroidal neovascularization, and diabetic retinopathy. circMET silencing could suppress pathological angiogenesis and tip cell specification via circMET/IGF2BP2/NRARP or ESM1 complex. circMET expression is increased in the vitreous samples of DR patients, and its silencing could suppress human diabetic

test. (C and D) HRVECs were transfected with negative control siRNA (si-NC), circMET siRNA1, or circMET siRNA2 for 24 h qRT-PCR assays (C) and western blots (D) were conducted to detect the levels of NRARP and ESM1 expression. n = 4; one-way ANOVA followed by Bonferroni's post hoc test. (E) RNA-FISH and immunofluorescence analysis was conducted to detect the co-localization of circMET/IGF2BP2/NRARP or ESM1. Scale bar: 50 μm. (F) RIP assay was conducted using IgG and IGF2BPs to detect the enrichment of NRARP or ESM1 in HRVECs transfected with negative siRNA, circMET siRNA1, circMET siRNA2, vector, or circMET. n = 4; one-way ANOVA followed by Bonferroni's post hoc test.

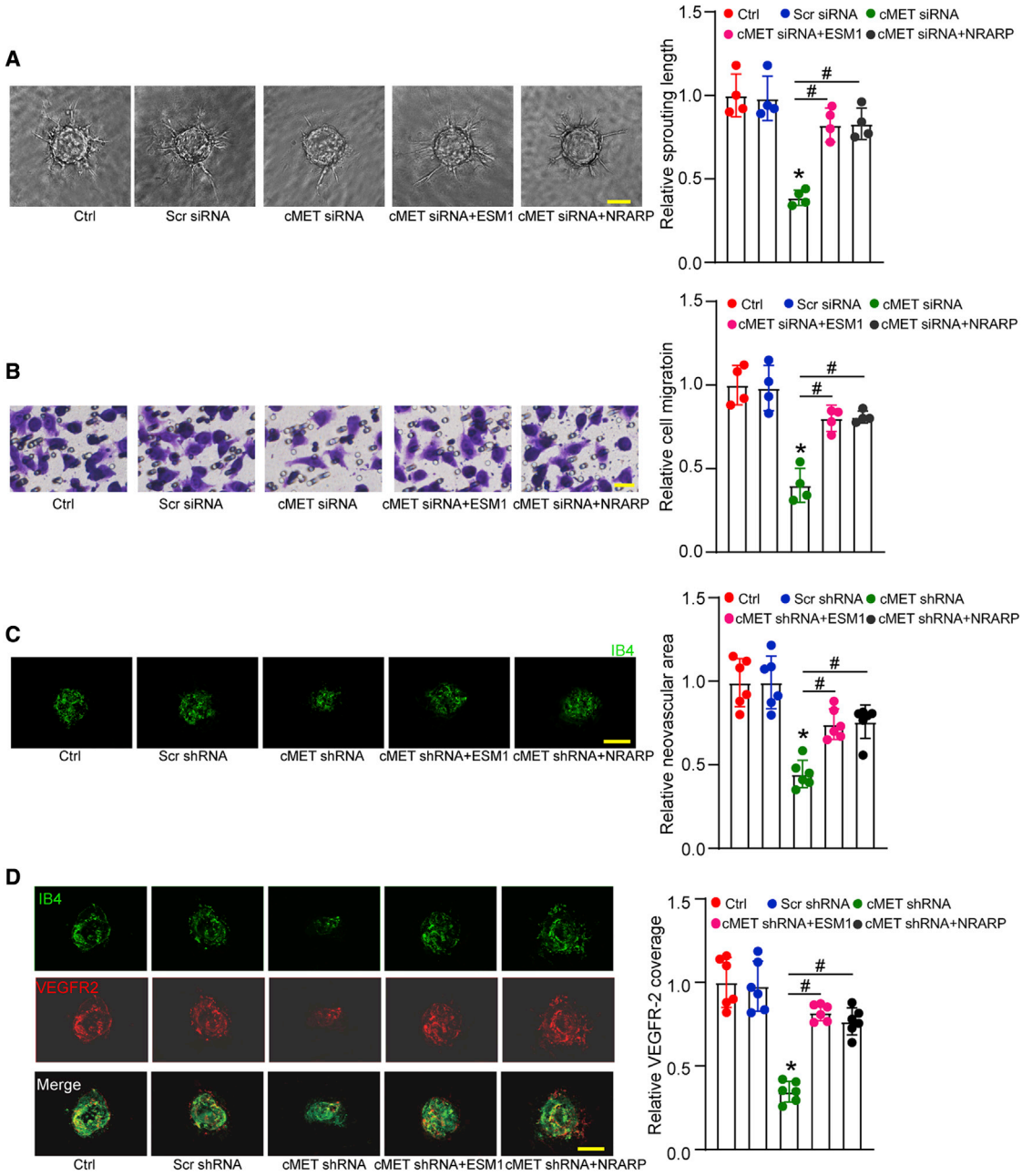

Figure 6. circMET regulates endothelial sprouting and pathological angiogenesis through NRARP/ESM1 pathway

(A and B) HRVECs were transfected as indicated for 24 h. *In vitro* spheroid sprouting assay and quantitative analysis was conducted to detect endothelial sprouting ability. Scale bar: 100 μm (A). Transwell assay and quantitative analysis conducted to detect endothelial cell migration. Scale bar: 50 μm (B). n = 4; one-way ANOVA followed by Bonferroni's post hoc test; *$p < 0.05$ versus Ctrl group; #$p < 0.05$ significant difference between the marked group. (C and D) RPE/choroid complexes were dissected and flat-mounted on day 14 after laser photocoagulation. The blood vessels were stained with IB-4 to show neovascular area. The representative images of IB-4 staining are shown. Scale bar: 50 μm (C). CNV lesions were stained with IB-4 and VEGFR2 to label choroidal neovascularization and vascular tip cells. Scale bar: 50 (D). n = 6 mice per group; Kruskal-Wallis test followed by Bonferroni's post hoc test.

vitreous-induced endothelial sprouting and pathological angiogenesis. These findings suggest that circMET is a therapeutic target for the treatment of proliferative retinopathies.

The specialization of tip and stalk cell plays an important role in many models of sprouting angiogenesis, including proliferative retinopathy.[4] During angiogenesis, some endothelial cells adopt a tip

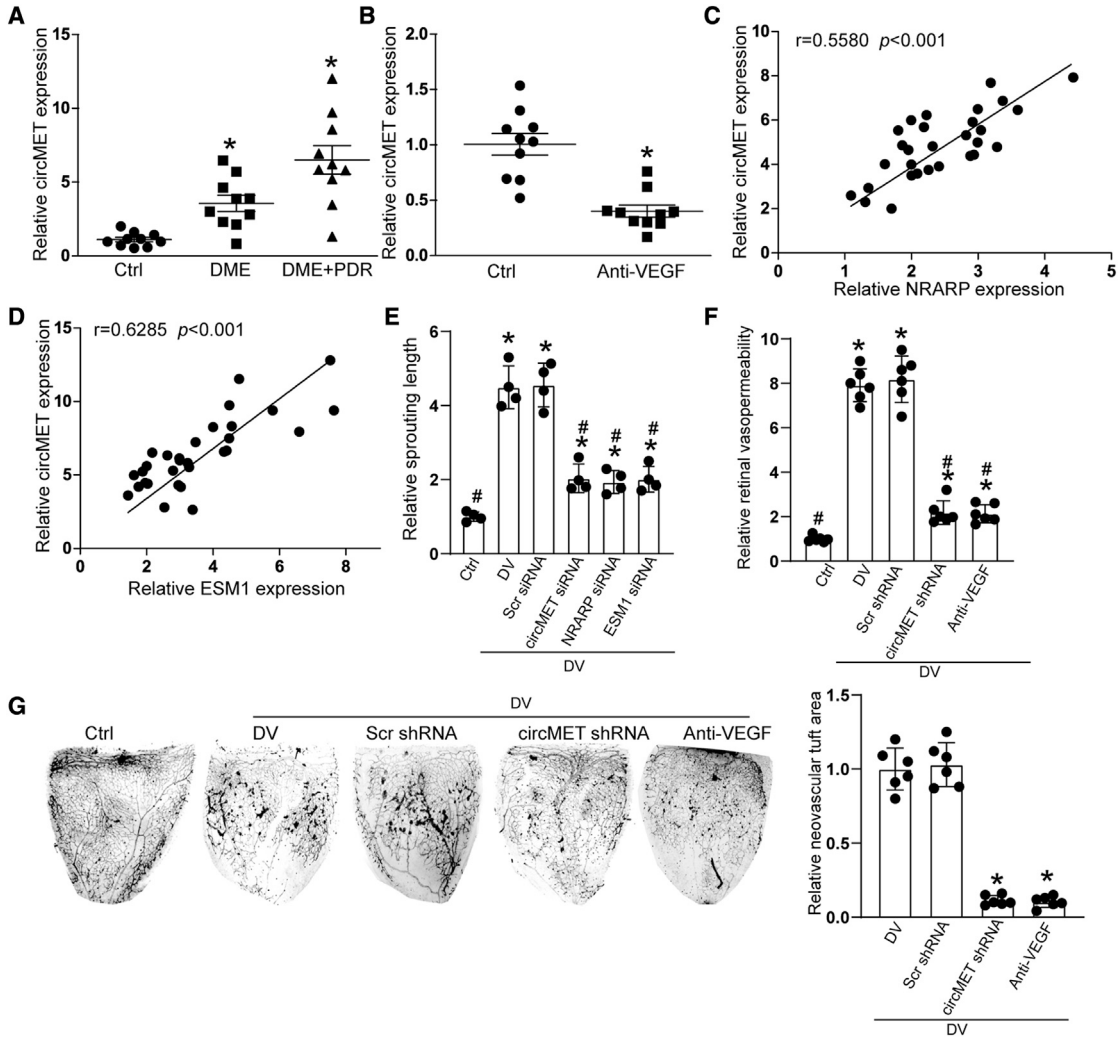

Figure 7. Clinical implication of circMET/NRARP or ESM1 signaling in ocular vascular dysfunction

(A) Human vitreous specimens were obtained from 30 subjects at the time of pars plana vitrectomy, including non-DR patients with macular holes (Ctrl, n = 10 eyes), patients with DME only (n = 10 eyes), and patients with DME and PDR (n = 10 eyes). qRT-PCRs were conducted to detect the level of circMET expression. *p < 0.05 versus Ctrl group, Kruskal-Wallis's test followed by Bonferroni's post hoc test. (B) Human vitreous specimens were obtained from 20 patients with PDR who received preoperative anti-VEGF treatment (n = 10 eyes) and did not receive anti-VEGF therapy (Ctrl, n = 10 eyes). qRT-PCRs were conducted to detect the expression level of circMET. Mann-Whitney *U* test. (C and D) The expression correlation between circMET and NRARP/ESM1 was analyzed using the patients with DR (n = 30 eyes). qRT-PCR was conducted to detect the expression level of circMET. ELISA assays were conducted to detect the expression of NRARP and ESM1. (E) HRVEC spheroids embedded in collagen were stimulated with diabetic vitreous (DV) without or with scramble shRNA (Scr shRNA), circMET siRNA, NRARP siRNA, or ESM1 siRNA for 24 h. Quantitative analysis of the mean sprout length was conducted on at least ten spheroids per experimental group. n = 4; *p < 0.05 versus Ctrl group, #p < 0.05 versus DV group. One-way ANOVA followed by Bonferroni's post hoc test. (F and G) EB evaluation of retinal vascular leakage in retinal extracts from the mice injected with PBS (Ctrl), diabetic vitreous without (DV) or with scramble shRNA (Scr shRNA), circMET shRNA, or anti-VEGF after 4 weeks of treatment (F, n = 6 retinas per group). Quantifications of retinal neovascular tufts were also conducted after 4 weeks of treatment (G, n = 6 retinas per group). *p < 0.05 versus Ctrl group, #p < 0.05 versus DV group, Kruskal-Wallis's test followed by Bonferroni's post hoc test.

phenotype and lead a new angiogenic branch. The stalk cells form the stalk of a branch and proliferate to form vessel lumen.[29,30] The levels of circMET are significantly upregulated in proliferative retinopathies. circMET silencing suppresses pathological angiogenesis and tip cell formation. In the normal development, tip cells play a tightly controlled and timely role in angiogenesis. By contrast, an excessive number of tip cells occur during chaotic and pathological angiogenesis in proliferative retinopathies. Previous studies have reported that circMET overexpression promotes hepatocellular carcinoma development by inducing the epithelial to mesenchymal transition.[31] circMET promotes non-small-cell lung cancer (NSCLC) cell proliferation, metastasis, and immune evasion.[32] Here, we reveal a similar role of circMET in retinal endothelial cells. Increased circMET contributes to endothelial migration and sprouting. We thus speculate

that the induction of circMET is a trigger factor of ocular angiogenesis.

circRNAs have been shown to be involved in the post-transcriptional regulation by acting as miRNA sponges or protein sponges.[16] circMET is not enriched by Ago2 antibody, suggesting that circMET cannot act as the miRNA sponge in HRVECs. We show that circMET enhances the stability of NRARP or ESM1 mRNA by forming a circMET/IGF2BP2/NRARP or ESM1 complex. IGF2BP2 is an *N*6-methyladenosine (m^6A) reader that participates in many biological processes by communicating with different RNA transcripts. They can regulate the stability of the target mRNAs in an m^6A-dependent manner.[33] m^6A modification is mainly mediated by methyltransferase-like 3 (METTL3) and methyltransferase-like 14 (METTL14) heterodimer.[34,35] The interaction between circMET and IGF2BP2 is remarkably impaired by METTL3/14 knockdown, suggesting that circMET physically interacts with IGF2BP2 in an m^6A-dependent manner.

NRARP gene encodes an ankyrin-repeat protein and acts as a molecular link between Notch- and Lef1-dependent Wnt in endothelial cells, which can coordinate Notch signaling and Wnt signaling to control vessel density in angiogenesis.[36,37] ESM-1 is a soluble endothelial cell proteoglycan, released by the damaged vascular endothelium upon inflammatory cytokines and angiogenic stimuli.[38,39] It can regulate endothelial tip cell behavior and vascular permeability by enhancing VEGF bioavailability. Based on the above-mentioned evidence, we conclude that NRARP and ESM-1 are important regulators of angiogenesis and tip cell behavior. During angiogenesis, the levels of circMET are significantly upregulated. The binding between circMET and IGF2BP2 can stabilize the expression of NRARP and ESM-1 mRNA. Continuous expression of NRARP and ESM-1 would promote the specification of tip cells and pathological angiogenesis.

Clinical evidence has revealed that circMET level is significantly upregulated in the vitreous of the patients with DME or PDR. The expression of circMET is tightly correlated with the severity of diabetes-induced retinal vascular complication. Moreover, anti-VEGF treatment could reduce the level of circMET expression. These results indicate that circMET is an indicator of pathogenic processes or pharmacologic responses to a therapeutic intervention, which can be used as a promising biomarker for the diagnosis and prognosis of retinal vascular complication. circMET silencing can counteract the effects of human diabetic vitreous-induced retinal vessel leak and decrease neovascular tuft area. VEGF and other endogenous factors that can drive angiogenesis have been studied in the past decades.[40] Currently, VEGF-A antagonists are the standard care in the treatment of retinal vascular diseases; however, a small number of patients have no clinical response or a delayed response to VEGF-A antagonists.[41,42] Tip cells have unique functional and molecular signatures and are attractive targets for therapeutic treatment of angiogenesis.[6] The inhibitor of circMET signaling that primarily targets tip cells can inhibit pathological angiogenesis in the retina efficiently and safely. Since the eye is a small and self-contained compartment,[43] high-level and region-restricted inhibition of circMET signaling may provide an alternative option for treating retinal vascular diseases.

In conclusion, we provide important evidence that circMET is a critical pro-angiogenic factor and a diagnostic/prognostic biomarker for ocular vascular disease. circMET exerts a critical role in stabilizing NRARP or ESM1 expression via the formation of circMET/IGF2BP2/NRARP or ESM1 complex to promote angiogenesis by targeting tip cell specialization. circMET is shown as a promising therapeutic target for in the treatment of proliferative retinopathies and other diseases associated with pathological angiogenesis.

MATERIALS AND METHODS

Ethics statement

All animals were maintained according to the guidelines of the Care and Use of Laboratory Animals (published by the National Institutes of Health, NIH publication no. 86-23, revised 1996). Animal experiments were conducted according to the guidelines of (ARVO) Statement for the Use of Animals in Ophthalmic and Vision Research and approved by the Animal Care and Use Committee of the authors' institute. The clinical samples were handled according to the Declaration of Helsinki. The relevant patients gave informed consent before inclusion.

Animals

Wild-type (WT) C57BL/6J mice were purchased from Nanjing Qinglongshan Experimental Animal Center (Nanjing, China). Cdh5-Cre mice, which were generated on the pure C57BL/6J background, were purchased from Beijing Biocytogen (Beijing, China). They were maintained under pathogen-free condition with a 12-h light-dark cycle and fed with standard laboratory chow and allowed ad libitum access to water.

Laser-induced CNV model

C57BL/6J mice (6–8 weeks old, male) were used to build the laser-induced CNV model. Briefly, they were anesthetized with ketamine (80 mg/kg) and xylazine (4 mg/kg). The pupils were dilated with an eye drop containing 0.5% phenylephrine and 0.5% tropicamide. Then, a coverslip with a drop of gel was placed on the eye as a contact lens to view the fundus. Bruch's membrane was ruptured at 3, 6, 9, and 12 o'clock positions using the OcuLight GLx Laser System (Iridex, USA). The laser parameters were set as follows: 577 nm wavelength, 50 μm spot size, 120 mW power, and 100 ms duration. The sign of an air bubble indicated the disruption of Bruch's membrane. Laser injury without hemorrhage was included.[20]

Oxygen-induced retinopathy model

Neonatal C57BL/6J mice and their nursing mother were exposed to 75% oxygen from P7 to P12. Then, these mice were returned to normoxic condition for 5 days, triggering hypoxia-induced vasoproliferation. Age-matched mice in room air were used as the controls.[44]

Induction of diabetes mellitus

C57BL/6 mice (8 weeks old, male) were fasted for 6 h before STZ (Sigma-Aldrich, USA) injection. They received an intraperitoneal

injection of STZ (50 mg/kg) or vehicle (citrate buffer control) for 5 consecutive days. The fasting blood glucose was detected by the One-Touch Ultra meter (LifeScan, USA) at 7 days after the last injection of STZ. The mice with glucose levels >15 mmol/L were considered the diabetic mice.[45]

Cell culture and transfection

HRVECs (passage 4–7) were cultured in EGM2-MV medium (CC-3202, Lonza, Switzerland) supplemented with 5% FBS and 1% antibiotic-antimycotic solution. They were incubated at 37°C, 5% CO_2, and 95% relative humidity. siRNAs directed against circMET and scramble siRNAs were synthesized by GenePharma (Shanghai, China). Lipofectamine 6000 (C0526, Beyotime, China) was used to introduce siRNAs into HRVECs at approximately 70% confluence according to the manufacturer's protocols.

Isolation and purification of murine retinal microvascular endothelial cells (RMECs) and pericytes

RMECs and pericytes were isolated from C57BL/6 mouse retinas by collecting retinas from one litter of mice (n = 6–7, 4 weeks old). The retinas (n = 12–14) were rinsed in the serum-free DMEM (11995065, Gibco, USA) containing penicillin/streptomycin 1%, pooled in a 60-mm dish, minced, and digested with 1.6 mg/mL Liberase DL (BE0002726, Roche, Belgium) and 0.1 mg/mL DNase I (90,083, Sigma-Aldrich, USA) in serum-free DMEM at 37°C for 45 min. The cell dissociation was filtered through 100-μm and 45-μm nylon filter, centrifuged for 5 min at 400 *g*, washed, and re-suspended with DMEM with 10% FBS to obtain the single cell suspension. The CD31-microBeads and NG2-microBeads were prepared by conjugating 10 μL magnetic Dynabeads (110.35, Invitrogen, USA) with CD31 antibody or NG2 antibody. The single cell suspension was re-suspended in 100 μL 2 mM PBS/EDTA and 0.5% BSA and incubated with CD31-microBeads or NG2-microBeads at 4°C for 20 min. Both RMECs and pericytes were isolated using a DynaMag magnet (12303D, Invitrogen, USA). The cell purity was assessed by immunofluorescence staining.

Statistics

Statistical analysis was conducted using GraphPad Prism 8. For the normally distributed data with equal variance, statistical analysis was conducted using two-tailed Student's t test (two-group comparisons) or one-way analysis of variance (ANOVA) followed by Bonferroni's post hoc test (multi-group comparisons) as appropriate. For non-normally distributed data or data with unequal variances, statistical analysis was conducted using nonparametric Mann-Whitney *U* test (two-group comparisons) or Kruskal-Wallis test followed by Bonferroni's post hoc test (multi-group comparisons). *$p < 0.05$ was considered statistically significant.

SUPPLEMENTAL INFORMATION

Supplemental information can be found online at https://doi.org/10.1016/j.ymthe.2022.01.012.

ACKNOWLEDGMENTS

We thank J. Yao, X.-M. Li, and H.-M. Ge (Nanjing Medical University, China) for the excellent technical and clinical assistance; Z.-H. Wang (College of Information, Shanghai Ocean University, China) for statistical discussion and the support of bioinformatics analysis. This work was generously supported by the grants from the National Natural Science Foundation of China (no.81770945 and 81970809 to Dr Yan; no. 81570859 and 82070983 to Dr Jiang), a grant from the Shanghai Youth Talent Support Program (to Dr Yan), a grant from the Scientific Research Start-up Funding for Advanced Talents (to Dr Yan).

AUTHOR CONTRIBUTIONS

B.Y., Q.J., and C.Z. designed research; M.D.Y., Q.Y.Z., Y.M., Y.Z., and Z.H.S. performed research; M.D.Y. and Q.Y.Z. analyzed data; B.Y. wrote the article.

DECLARATION OF INTERESTS

The authors declare no competing interests.

REFERENCES

1. Potente, M., Gerhardt, H., and Carmeliet, P. (2011). Basic and therapeutic aspects of angiogenesis. Cell *146*, 873–887.
2. Li, X., Sun, X., and Carmeliet, P. (2019). Hallmarks of endothelial cell metabolism in health and disease. Cell Metab. *30*, 414–433.
3. Cao, R., Xue, Y., Hedlund, E.M., Zhong, Z., Tritsaris, K., Tondelli, B., Lucchini, F., Zhu, Z., Dissing, S., and Cao, Y. (2010). VEGFR1-mediated pericyte ablation links VEGF and PlGF to cancer-associated retinopathy. Proc. Natl. Acad. Sci. U S A *107*, 856–861.
4. Chen, W., Xia, P., Wang, H., Tu, J., Liang, X., Zhang, X., and Li, L. (2019). The endothelial tip-stalk cell selection and shuffling during angiogenesis. J. Cell Commun. Signal. *13*, 291–301.
5. Margadant, C. (2020). Positive and negative feedback mechanisms controlling tip/stalk cell identity during sprouting angiogenesis. Angiogenesis *23*, 75–77.
6. Eilken, H.M., and Adams, R.H. (2010). Dynamics of endothelial cell behavior in sprouting angiogenesis. Curr. Opin. Cell Biol. *22*, 617–625.
7. Cao, R., Jensen, L.D., Söll, I., Hauptmann, G., and Cao, Y. (2008). Hypoxia-induced retinal angiogenesis in zebrafish as a model to study retinopathy. PLoS One *3*, e2748.
8. Ali, Z., Cui, D., Yang, Y., Tracey-White, D., Vazquez-Rodriguez, G., Moosajee, M., Ju, R., Li, X., Cao, Y., and Jensen, L.D. (2020). Synchronized tissue-scale vasculogenesis and ubiquitous lateral sprouting underlie the unique architecture of the choriocapillaris. Dev. Biol. *457*, 206–214.
9. Siemerink, M.J., Klaassen, I., Van Noorden, C.J., and Schlingemann, R.O. (2013). Endothelial tip cells in ocular angiogenesis: potential target for anti-angiogenesis therapy. J. Histochem. Cytochem. *61*, 101–115.
10. Liu, Z., Yan, S., Wang, J., Xu, Y., Wang, Y., Zhang, S., Xu, X., Yang, Q., Zeng, X., Zhou, Y., et al. (2017). Endothelial adenosine A2a receptor-mediated glycolysis is essential for pathological retinal angiogenesis. Nat. Commun. *8*, 1–18.
11. Al-Latayfeh, M., Silva, P.S., Sun, J.K., and Aiello, L.P. (2012). Antiangiogenic therapy for ischemic retinopathies. Cold Spring Harb. Perspect. Med. *2*, a006411.
12. Miller, J.W., Le Couter, J., Strauss, E.C., and Ferrara, N. (2013). Vascular endothelial growth factor a in intraocular vascular disease. Ophthalmology *120*, 106–114.
13. Zhang, F., Tang, Z., Hou, X., Lennartsson, J., Li, Y., Koch, A.W., Scotney, P., Lee, C., Arjunan, P., Dong, L., et al. (2009). VEGF-B is dispensable for blood vessel growth but critical for their survival, and VEGF-B targeting inhibits pathological angiogenesis. Proc. Natl. Acad. Sci. U S A *106*, 6152–6157.
14. Kaikkonen, M.U., Lam, M.T., and Glass, C.K. (2011). Non-coding RNAs as regulators of gene expression and epigenetics. Cardiovasc. Res. *90*, 430–440.

15. Taft, R.J., Pang, K.C., Mercer, T.R., Dinger, M., and Mattick, J.S. (2010). Non-coding RNAs, regulators of disease. J. Pathol. *220*, 126–139.

16. Salzman, J. (2016). Circular RNA expression: its potential regulation and function. Trends Genet. *32*, 309–316.

17. Shao, T., Pan, Y.H., and Xiong, X.D. (2020). Circular RNA, an important player with multiple facets to regulate its parental gene expression. Mol. Ther. Nucleic Acids *23*, 369–376.

18. Ashwal-Fluss, R., Meyer, M., Pamudurti, N.R., Ivanov, A., Bartok, O., Hanan, M., Evantal, N., Memczak, S., Rajewsky, N., and Kadener, S. (2014). circRNA biogenesis competes with pre-mRNA splicing. Mol. Cell *56*, 55–66.

19. Han, B., Chao, J., and Yao, H. (2018). Circular RNA and its mechanisms in disease: from the bench to the clinic. Pharmacol. Ther. *187*, 31–44.

20. Lambert, V., Lecomte, J., Hansen, S., Blacher, S., Gonzalez, M.L., Struman, I., Sounni, N.E., Rozet, E., de Tullio, P., Foidart, J.M., et al. (2013). Laser-induced choroidal neovascularization model to study age-related macular degeneration in mice. Nat. Protoc. *8*, 2197–2211.

21. del Toro, R., Prahst, C., Mathivet, T., Siegfried, G., Kaminker, J.S., Larrivee, B., Breant, C., Duarte, A., Takakura, N., Fukamizu, A., et al. (2010). Identification and functional analysis of endothelial tip cell-enriched genes. Blood *116*, 4025–4033.

22. Kim, Y., and Kim, V.N. (2012). MicroRNA factory: RISC assembly from precursor microRNAs. Mol. Cell. *25*, 384–386.

23. Liu, C., Yao, M.D., Li, C.P., Shan, K., Yang, H., Wang, J.J., Liu, B., Li, X.M., Yao, J., Jiang, Q., and Yan, B. (2017). Silencing of circular RNA-ZNF609 ameliorates vascular endothelial dysfunction. Theranostics *8*, 2863–2877.

24. Zhou, K.I., and Pan, T. (2018). An additional class of m^{6}A readers. Nat. Cell Biol. *20*, 230–232.

25. Huang, H., Weng, H., Sun, W., Qin, X., Shi, H., Wu, H., Zhao, B.S., Mesquita, A., Liu, C., Yuan, C.L., et al. (2018). Recognition of RNA N^6-methyladenosine by IGF2BP proteins enhances mRNA stability and translation. Nat. Cell Biol. *20*, 285–295.

26. Dai, N. (2020). The diverse functions of IMP2/IGF2BP2 in metabolism. Trends Endocrinol. Metab. *31*, 670–679.

27. Jensen, L.D., Nakamura, M., Bräutigam, L., Li, X., Liu, Y., Samani, N.J., and Cao, Y. (2015). VEGF-B-Neuropilin-1 signaling is spatiotemporally indispensable for vascular and neuronal development in zebrafish. Proc. Natl. Acad. Sci. U S A *112*, E5944–E5953.

28. Rajappa, M., Saxena, P., and Kaur, J. (2010). Ocular angiogenesis: mechanisms and recent advances in therapy. Adv. Clin. Chem. *50*, 103–121.

29. Jakobsson, L., Franco, C.A., Bentley, K., Collins, R.T., Ponsioen, B., Aspalter, I.M., Rosewell, I., Busse, M., Thurston, G., Medvinsky, A., et al. (2010). Endothelial cells dynamically compete for the tip cell position during angiogenic sprouting. Nat. Cell Biol. *12*, 943–953.

30. Boareto, M., Jolly, M.K., Ben-Jacob, E., and Onuchic, J.N. (2015). Jagged mediates differences in normal and tumor angiogenesis by affecting tip-stalk fate decision. Proc. Natl. Acad. Sci. U S A *112*, E3836–E3844.

31. Huang, X.Y., Zhang, P.F., Wei, C.Y., Peng, R., Lu, J.C., Gao, C., Cai, J.B., Yang, X., Fan, J., Ke, A.W., et al. (2020). Circular RNA circMET drives immunosuppression and anti-PD1 therapy resistance in hepatocellular carcinoma via the miR-30-5p/snail/DPP4 axis. Mol. Cancer *19*, 1–18.

32. Pei, X., Chen, S.W., Long, X., Zhu, S.Q., Qiu, B.Q., Lin, K., Lu, F., Xu, J.J., Zhang, P.F., and Wu, Y.B. (2020). circMET promotes NSCLC cell proliferation, metastasis, and immune evasion by regulating the miR-145-5p/CXCL3 axis. Aging (Albany NY) *12*, 13038–13058.

33. Hu, X., Peng, W.X., Zhou, H., Jiang, J., Zhou, X., Huang, D., Mo, Y.Y., and Yang, L. (2020). IGF2BP2 regulates DANCR by serving as an *N*6-methyladenosine reader. Cell Death Differ *27*, 1782–1794.

34. Cao, G., Li, H.B., Yin, Z., and Flavell, R.A. (2016). Recent advances in dynamic m^{6}A RNA modification. Open Biol. *6*, 160003.

35. Dai, F., Wu, Y., Lu, Y., An, C., Zheng, X., Dai, L., Guo, Y., Zhang, L., Li, H., Xu, W., et al. (2020). Crosstalk between RNA m^{6}A modification and non-coding RNA contributes to cancer growth and progression. Mol. Ther. Nucleic Acids *22*, 62–71.

36. Jarrett, S.M., Seegar, T.C., Andrews, M., Adelmant, G., Marto, J.A., Aster, J.C., and Blacklow, S.C. (2019). Extension of the Notch intracellular domain ankyrin repeat stack by NRARP promotes feedback inhibition of Notch signaling. Sci. Signal. *12*, eaay2369.

37. Pinto, I., Duque, M., Gonçalves, J., Akkapeddi, P., Oliveira, M.L., Cabrita, R., Yunes, J.A., Durum, S.K., Barata, J.T., and Fragoso, R. (2020). NRARP displays either pro-or anti-tumoral roles in T-cell acute lymphoblastic leukemia depending on Notch and Wnt signaling. Oncogene *39*, 975–986.

38. Sun, H., Zhang, H., Li, K., Wu, H., Zhan, X., Fang, F., Qin, Y., and Wei, Y. (2019). ESM-1 promotes adhesion between monocytes and endothelial cells under intermittent hypoxia. J. Cell Physiol. *234*, 1512–1521.

39. Rocha, S.F., Schiller, M., Jing, D., Li, H., Butz, S., Vestweber, D., Biljes, D., Drexler, H.C., Nieminen-Kelhä, M., Vajkoczy, P., et al. (2014). Esm1 modulates endothelial tip cell behavior and vascular permeability by enhancing VEGF bioavailability. Circ. Res. *115*, 581–590.

40. Gacche, R.N., and Meshram, R.J. (2014). Angiogenic factors as potential drug target, efficacy and limitations of anti-angiogenic therapy. Biochim. Biophys. Acta *1846*, 161–179.

41. Quaggin, S.E. (2012). Turning a blind eye to anti-VEGF toxicities. J. Clin. Invest. *122*, 3849–3851.

42. Campochiaro, P.A. (2019). Low risk to retina from sustained suppression of VEGF. J. Clin. Invest. *129*, 3029–3031.

43. Jiang, Q., Liu, C., Li, C.P., Xu, S.S., Yao, M.D., Ge, H.M., Sun, Y.N., Li, X.M., Zhang, S.J., Shan, K., et al. (2020). Circular RNA-ZNF532 regulates diabetes-induced retinal pericyte degeneration and vascular dysfunction. J. Clin. Invest. *130*, 3833–3847.

44. Scott, A., and Fruttiger, M. (2010). Oxygen-induced retinopathy, a model for vascular pathology in the retina. Eye (Lond) *24*, 416–421.

45. Shan, K., Liu, C., Liu, B.H., Chen, X., Dong, R., Liu, X., Zhang, Y.Y., Liu, B., Zhang, S.J., Wang, J.J., et al. (2017). Circular noncoding RNA HIPK3 mediates retinal vascular dysfunction in diabetes mellitus. Circulation *136*, 1629–1642.

YMTHE, Volume *30*

Supplemental Information

Targeting circular RNA-MET for anti-angiogenesis treatment via inhibiting endothelial tip cell specialization

Mu-Di Yao, Qin Jiang, Yan Ma, Yan Zhu, Qiu-Yang Zhang, Ze-Hui Shi, Chen Zhao, and Biao Yan

Supplemental data

Supplemental Figure 1: Hypoxia leads to increased circMET expression

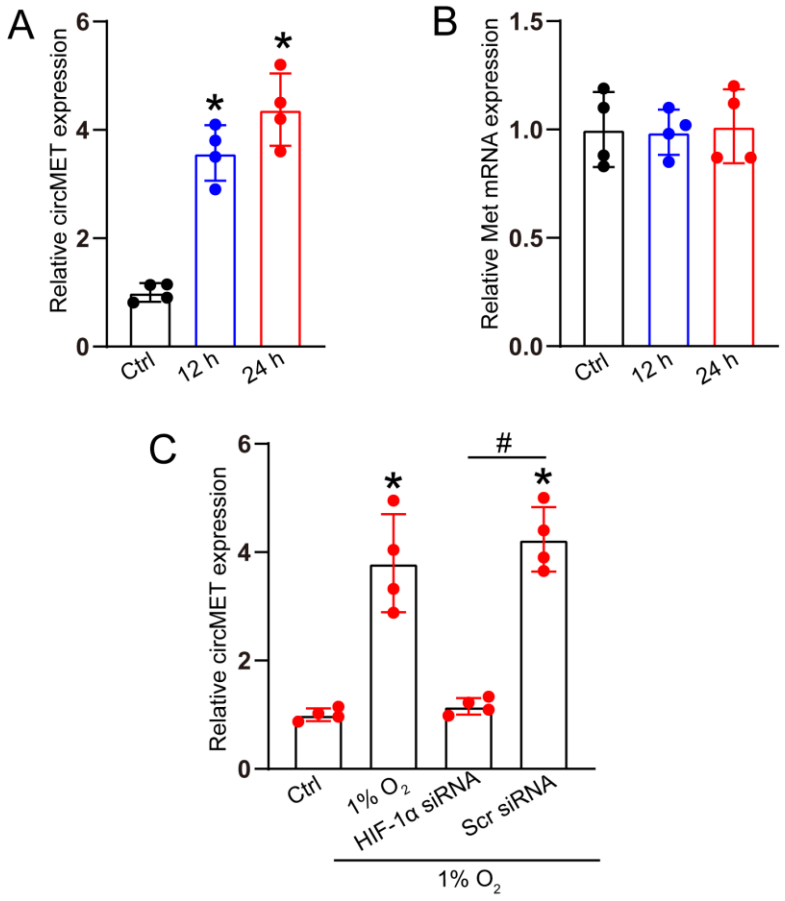

(A and B) HRVECs were exposed to hypoxia (1% O_2) for 12 h or 24 h. The group cultured in normoxia were taken as the control (Ctrl). qRT-PCRs were conducted to detect the expression pattern of circMET and MET mRNA (n = 4; One-way ANOVA followed by Bonferroni's post hoc test; $^{*}P < 0.05$ versus Ctrl). (C) HRVECs were transfected with HIF-1α siRNA, scramble (Scr) siRNA, or left untreated for 12 h, and then exposed to hypoxia (1% O_2) for 24 h. The group cultured in normoxia were taken as the control. qRT-PCRs were conducted to detect the expression pattern of circMET (n = 4; One-way ANOVA followed by Bonferroni's post hoc test; $^{*}P < 0.05$ versus Ctrl; $^{\#}P < 0.05$ between the marked groups).

Supplemental Figure 2: Injection of circMet shRNA leads to decreased circMet expression

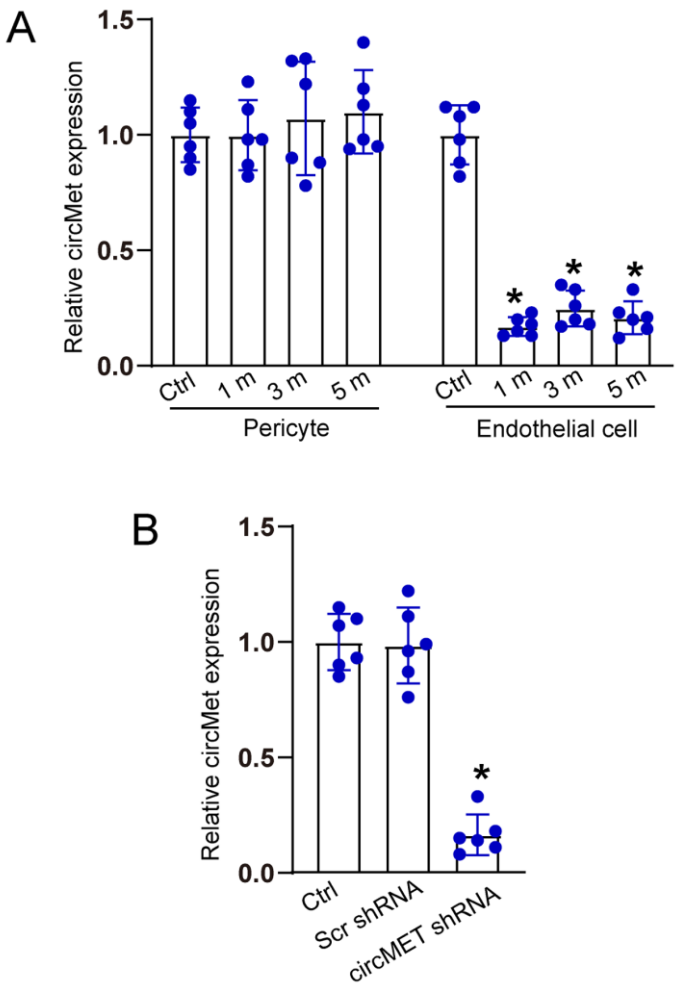

(A) circMet expression was detected by qRT-PCRs in the primarily isolated pericytes and endothelial cells from the retinas of Cdh5-Cre mice at 1-month, 3-month, and 5-month after Cre-dependent circMet shRNA administration. The pericytes or endothelial cells from Cdh5-Cre mice without Cre-dependent Cdh5-Cre shRNA administration were used as the control group (n = 6 mice per group). (B) circMet expression was determined by qRT-PCRs in choroidal complex at 2-week after subretinal injection of circMET shRNA, scramble (Scr) shRNA, or left untreated (Ctrl) in Cdh5-Cre mice. n = 6 mice per group. The significant difference was evaluated by Kruskal-Wallis's test followed by post hoc Bonferroni's test; *P<0.05.

Supplemental Figure 3: Transfection of circMET siRNA reduces circMET expression in HRVECs

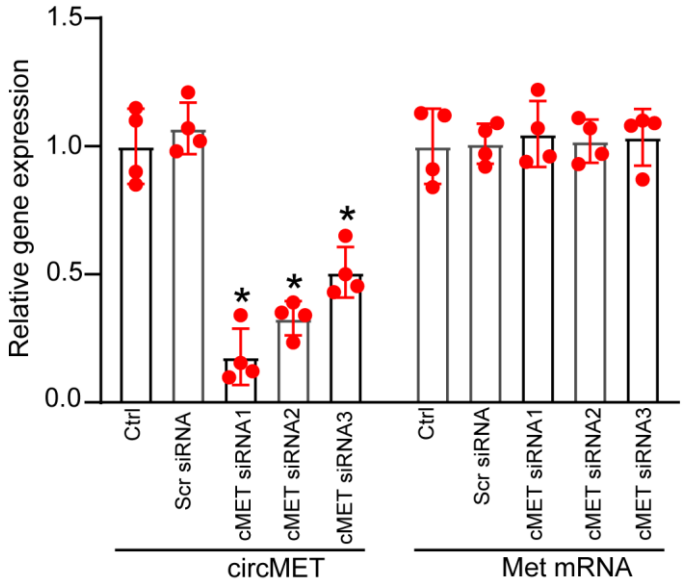

HRVECs were transfected with scrambled (Scr) siRNA, siRNA targeting the backsplice sequence of circMET (siRNA1, siRNA2 or siRNA3), or left untreated (Ctrl) for 48 hours. qRT-PCRs were conducted to detect the expression of circMET and Met mRNA (n = 4 biologically independent samples). The significant difference was evaluated by one-way ANOVA followed by Bonferroni's post-hoc test; *P<0.05.

Supplemental Figure 4: Transfection of circMET overexpression vector leads to increased circMET expression in HRVECs and choroid explants

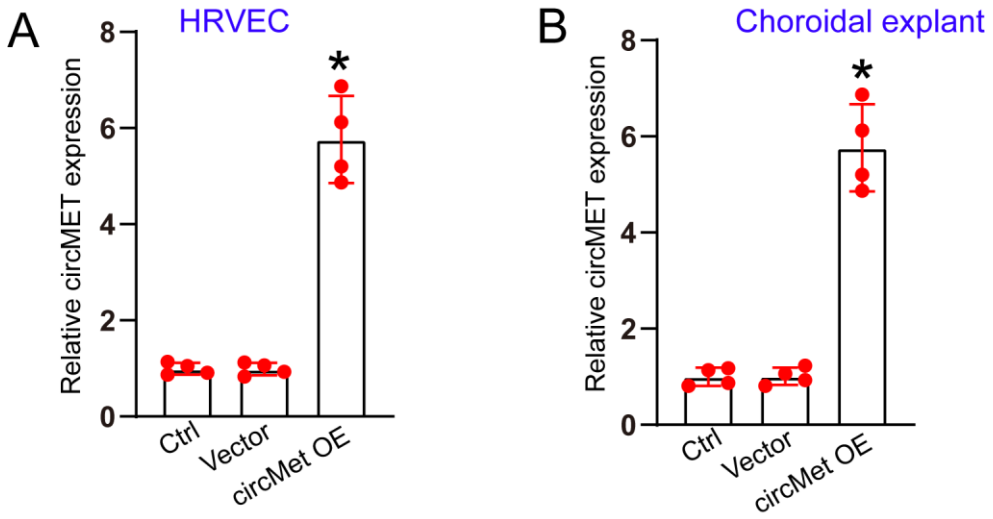

(A) HRVECs were transfected with null vector (Vector), circMet overexpression vector (circMet), or left untreated (Ctrl) for 24 hours. qPCR assays were conducted to detect the expression of circMet. n = 4; 1-way ANOVA followed by Bonferroni's post-hoc test, *P <0.05 versus Ctrl group. (B) Cdh5-Cre mice received a subretinal injection of null vector, circMet overexpression vector, or left untreated (Ctrl). Two days after injection, qPCR assays were conducted to detect the expression of circMet in the choroid explants. n = 4; *P <0.05 versus Ctrl group; 1-way ANOVA followed by Bonferroni's post hoc test.

Supplemental Figure 5: circMET overexpression affects endothelial tip cell specialization in vitro

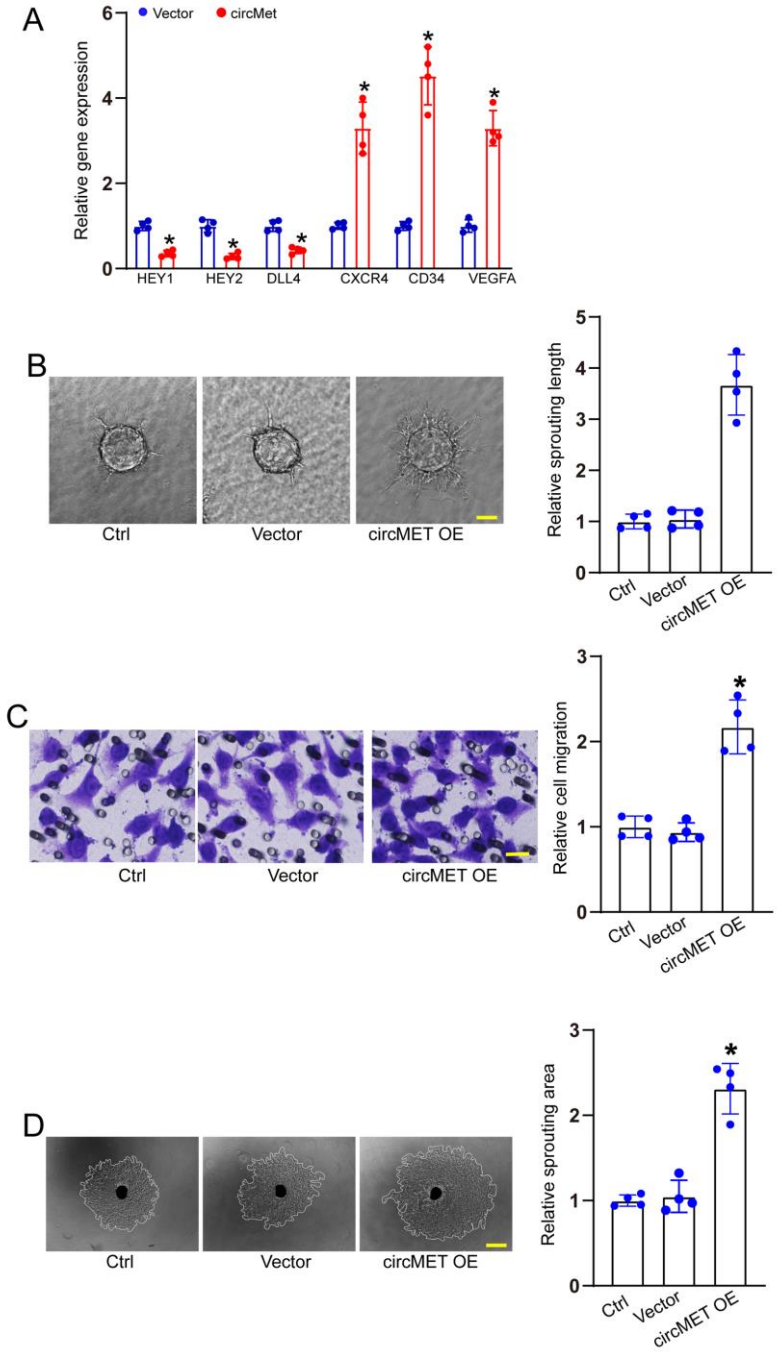

(A) HRVECs were transfected with null vector (Vector) or circMet overexpression vector (circMet) for 24 hours. qPCR assays were conducted to detect the expression of CXCR4, CD34, VEGFA, HEY1, HEY2, and DLL4. n = 4; Student *t* test; **P* <0.05 versus Vector group. (B) HRVECs were transfected with null vector, circMet overexpression vector (circMet), or left untreated (Ctrl) for 24 hours. In vitro spheroid sprouting assay and quantitative analysis was conducted to detect the role of circMet in endothelial sprouting ability. Scale bar: 20 μm. n = 4; 1-way ANOVA followed by Bonferroni's post-hoc test; **P* <0.05 versus Ctrl group. (C) Transwell assay and

quantitative analysis conducted to determine the effects of circMet overexpression on endothelial migration. Scale bar: 50 μm. n = 4; 1-way ANOVA followed by Bonferroni's post-hoc test; *P <0.05 versus Ctrl group. (D) Cdh5-Cre mice received a subretinal injection of negative control virus (Vector), circMet overexpression virus, or left untreated (Ctrl). On day 14, RPE/choroid complexes were dissected. The peripheral regions of RPE complexes were cut into 1mm × 1 mm pieces and seeded. The sprouting ability of choroidal explants was photographed on day 7. The representative images and quantification results of choroidal sprouting were shown. Scale bar: 500 μm. n = 4; *P <0.05 versus Ctrl group; 1-way ANOVA followed by Bonferroni's post hoc test.

Supplemental Figure 6: circMET does not act as a miRNA sponge in HRVECs

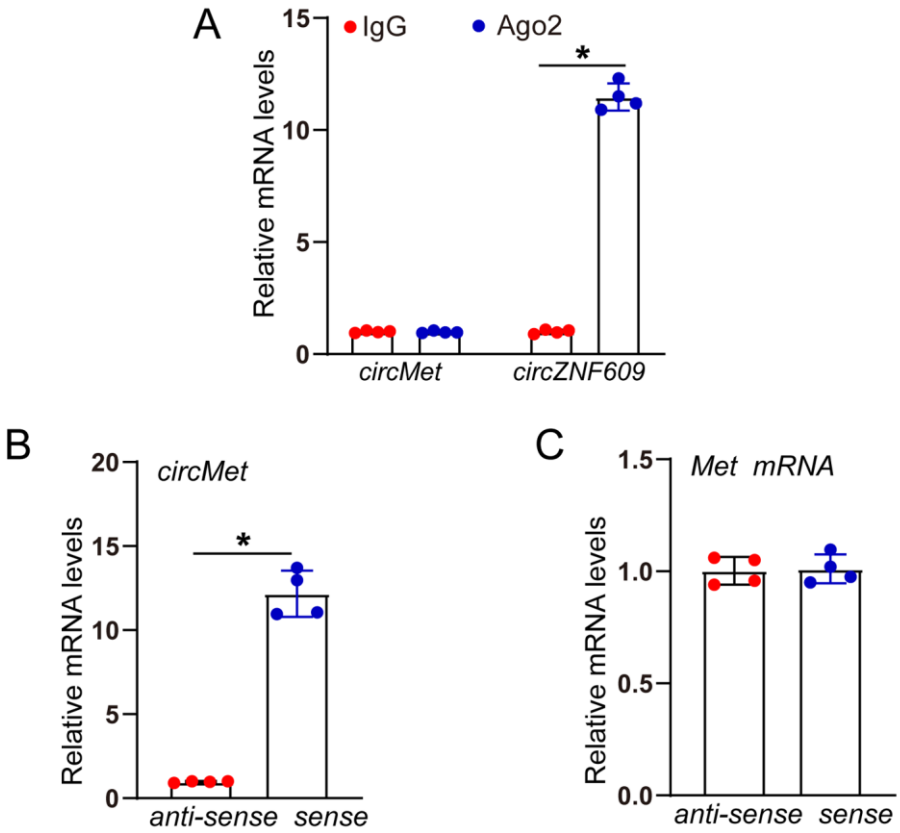

(A) Analysis for circMet and cicZNF609 enrichment, relative to IgG. RIP assays were conducted using Ago2 antibody or IgG in HRVECs transfected with Flag-Ago2 plasmid. n = 4. (B and C) RNA pull down assays were conducted to detect circMet (B) and Met mRNA (C) enrichment using the biotinylated sense probe which targeted the circMet back-splice junction region. n = 4. The significant difference was evaluated by student's *t* test.

Supplemental Figure 7: IGF2BP2 overexpression affects the stability of m^{6}A-modified circMET

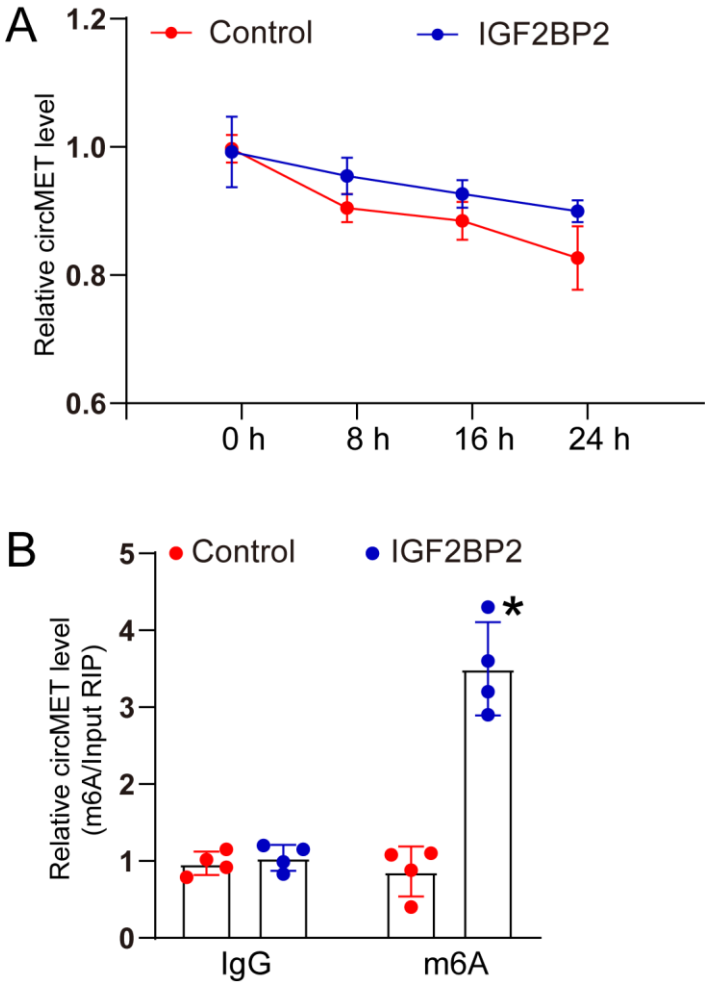

(A) Total RNAs from HRVECs were isolated at the indicated time points after the treatment with dimethyl sulfoxide (DMSO; Sigma; Ctrl) or Actinomycin D (2 mg/mL; Sigma) to constrain transcription. qRT-PCRs wereconducted to detect the levels of circMet (n = 4). (B) MeRIP-PCR assays were conducted to detect the levels of circMet in HRVECs transfected with IGF2BP2 overexpression vector and null vector (Ctrl). n = 4; *$P < 0.05$; Student's *t*-test.

Supplemental Figure 8: circMET overexpression leads to continuous expression of ESM1 and NRARP

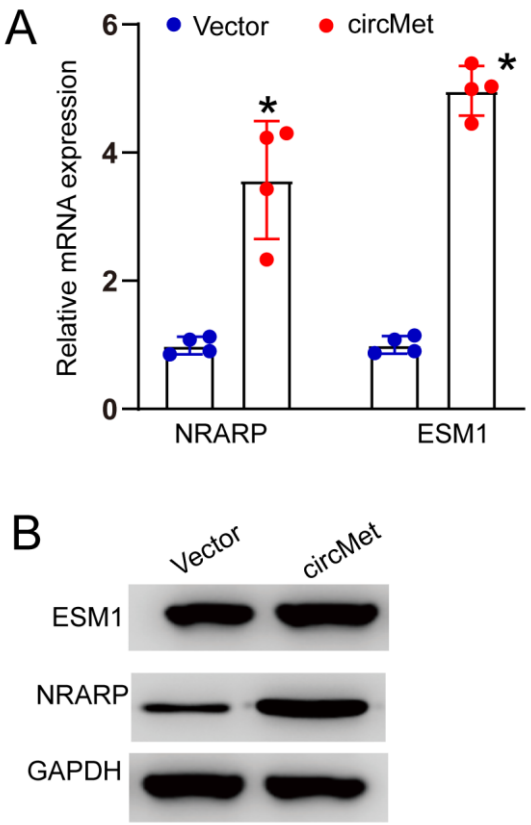

(A and B) HRVECs were transfected with null vector or circMet overexpression vector for 24 hours. qRT-PCR assays (A) and western blots (B) were conducted to detect the levels of NRARP and ESM1 expression. n = 4; $*P < 0.05$; Student's *t* test.

Supplemental Figure 9: IGF2BP2 interacts with ESM1 or NRARP in HRVECs

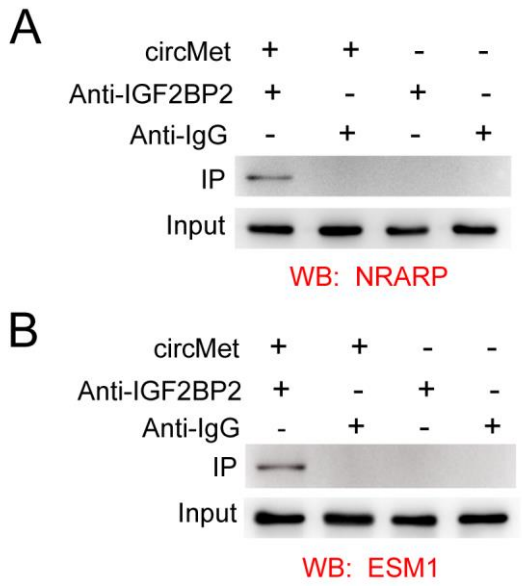

(A and B) The lysates of wild-type and circMET$^{-/-}$ HRVECs were subject for immunoprecipitation using IgG or IGF2BP2 antibody. The immunoprecipitates were then blotted with the indicated antibodies.

Supplemental materials and methods

Cell migration assay

Transwell assays were conducted to detect cell migration. Briefly, the transwell chamber with 8.0-μm pores (Corning, USA) was placed on a 24-well plate. HRVECs were plated into the upper chamber. DMEM supplemented with 10% FBS was added to the lower chamber as the chemoattractant. After migration, these non-migrated cells were removed and the filters were stained with the crystal violet to label the migrated cells.

Quantitative reverse transcription polymerase chain reaction (qRT-PCR)

Total RNA was extracted using TRIzol reagent (15596-026, Life Technologies, USA). About 1.5 mg of total RNAs were reversely transcribed into cDNAs using the SuperScript First Strand cDNA System (Invitrogen) according to the manufacturer's instructions. qRT-PCR assays were conducted using SYBR Green SuperMix (Roche). PCR amplification were performed for 45 cycles of 95°C for 30 s, 60°C for 30 s, and 72°C for 30 s with 1.0 μl of cDNA and SYBR Green Real-time PCR Master Mix (RR820A, Takara, Japan). Relative gene expression was determined by the $2^{-\Delta\Delta Ct}$ method.

Western blotting

Tissues or cells were rinsed with cold PBS and harvested in the lysis buffer. Equal amounts of lysates were separated on SDS-PAGE gels and transferred onto the PVDF membrane. The membranes were blocked in Tris-buffered saline containing 0.1% Tween and 5% skim milk for 3 hours at room temperature. Then, the membrane

was incubated with the primary antibody at 4 °C overnight and subsequently incubated with the secondary antibody at room temperature for 3 hours. The signals were visualized by the Pierce ECL Western Blotting Substrate (32209, Thermo Fisher Scientific, USA).

RNA fluorescence in situ hybridization (FISH)

The oligonucleotide-modified probe sequence for circMet was synthesized by Sangon Biotech (Shanghai, China). The fixed cells were washed in PBS and treated with RNase R at 37 °C for 15 min. The cell suspension was pipetted onto the glass slides, followed by dehydration with 70, 80 and 100% ethanol and hybridization at 37 °C overnight in a dark moist chamber. Then, the cells were denatured in 70% formamide/2×SSC, and incubated with fluorescence-labeled probes overnight. Finally, they were counterstained with DAPI for nuclei. The images were acquired by a fluorescence microscopy (Olympus, Japan). Pearson's correlation coefficient was analyzed by OLYMPUS FV1000 software.

RNA pull down assay

The biotin-labeled RNAs were transcribed using the Biotin RNA Labeling Mix (Roche Diagnostics) and T7 RNA polymerase (Roche Diagnostics), treated with RNase-free DNase I (4716728001, Roche, Belgium), and purified with an RNeasy Mini Kit (74104, Qiagen, USA). The biotin-coupled RNA complex was pulled down by incubating cell lysates with streptavidin-coated magnetic beads (88817, Thermo Scientific, USA). The retrieved proteins were determined by western blots. The bound proteins were eluted from the packed beads and analyzed by SDS-PAGE. The

enrichment of circMet or target mRNAs in the capture fractions was determined by qRT-PCR assays.

Spheroid formation assay

A total of 1×10^5 HRVECs were added to each well of a 96 -well suspension plate (Corning, USA) in 150 μl of endothelial cell (EC) growth medium-2 (EGM-2) (CC-3202, Lonza, Switzerland). They were allowed for the formation of spheroids overnight at 37 °C. Then, the spheroids were suspended, deposited over the first layer, and incubated at 37 °C for 2 hours. After the collagen gels were set, 100 μl of DEME medium containing 5% FBS was added to each well and the spheroids formed sprouts. After 24 hours, in vitro angiogenesis was quantitated by measuring the length and number of the sprouts that had grown out of each spheroid.

RNA-binding protein immunoprecipitation (RIP)

RIP assays were conducted using the Magna RIP™ RNA-Binding Protein Immunoprecipitation Kit (Millipore, USA) according to the protocol. HRVECs were incubated with RIP buffer containing the magnetic beads conjugated with Ago2 antibody, IGF2BPs antibody, or negative control IgG, and then lysed in the RIP lysis buffer. The immunoprecipitated RNAs were purified and the levels of target genes were detected by the quantitative PCR assays.

Plasmid construction

To overexpress the circMet and mutant circMet (circMet-MUT), the full sequences of circMet and mutant circMet were synthesized by GenePharma and cloned into the pcDNA3.1 (+) circRNA mini vector (60648, Addgene, USA) using the

EcoRV and SacII sites. The empty vector was used as the negative control. The transfection was performed using Lipofectamine 6000 (C0526, Beyotime, China) according to the manufacturer's protocols.

Immunoprecipitation assay

HRVECs were lysed in RIPA buffer (Beyotime, Shanghai, China) supplemented with the protease inhibitor cocktail (Sigma-Aldrich). The cell lysates were centrifuged at 12,000 g for 15 min. Then, the supernatant was subjected for immunoprecipitation with the corresponding antibody conjugated beads. After incubation at 4 °C overnight, the beads were washed twice in IP buffer and boiled in sodium dodecyl sulfate (SDS) sample buffer. Finally, the immunoprecipitates were subjected for western blots to detect protein-protein interaction.

Vitreous sample preparation

Vitreous samples were collected from the subjects undergoing pars plana vitrectomy for the treatment of DR and macular holes. All patients gave the informed consent before inclusion. Inclusion criteria for patients included the diagnosis of diabetes and the presence of ME or PDR. Exclusion criteria for the patients included non-diabetes or other ischemic retinal diseases. Vitreous samples from patients with ME or PDR were taken as the experimental group. Vitreous samples from non-diabetic patients for the treatment of macular hole were taken as control group. Vitreous samples were collected, placed immediately on ice, centrifuged for 15 min to remove insoluble materials, and stored at 80°C until use.

Immunofluorescence staining of choroidal flat-mount

The eyes were fixed in 4% paraformaldehyde for 30 min at room temperature and then dissected to obtain RPE/choroid complexes. After washing with PBS three times, the complexes were cut into four quadrants and flat mounted on glass slides. Subsequently, they were permeabilized and blocked with 5% BSA at 37℃ for 30 min. To visualize the neovascular area, they were incubated with Isolectin-B4 (1:50, L2895, Sigma-Aldrich) overnight at 4°C. Endothelial tip cells were observed by staining with Isolectin-B4 and VEGFR2 (1:300, sc-6251, Santa Cruz). Images were captured using a fluorescence microscope (Olympus, Tokyo, Japan) and analyzed by Image J software.

Immunofluorescence staining of retinal flat-mount

At P12 and P17, the mice were sacrificed and the eyes were enucleated. Following fixation in 4% paraformaldehyde for 0.5 hour, the eyes were dissected and the whole-mount retinas were obtained. The whole-mount retinas were washed three times with PBS before being permeabilized and blocked with 5% BSA for 45 min. Then, they were incubated with Isolectin-B4 (1:50, L2895, Sigma-Aldrich) overnight at 4℃ to visualize vascular networks. The images were captured using a fluorescence microscope (Olympusn) and analyzed with Image J.

Choroidal sprouting assay ex vivo

On day 14 post laser photocoagulation, the mice were killed and the eyes were immediately enucleated and kept in ice-cold DMEM medium. RPE/choroid complexes were isolated and cut into approximately 1 × 1 mm^2 pieces and embedded in 50 μL growth factor-reduced Matrigel (354230, Corning, USA) in 24-well plates.

The explants were grown in DMEM containing 10% FBS (16140071, Gibco, USA) and 1% Penicillin/Streptomycin (15140122, Gibco, USA) at 37°C with 5% CO_2. Endothelial sprouting images were taken by a light microscope (Olympus, Japan) and quantified by Image J software.

Endothelial conditional knockdown of circMet

Cre-dependent AAV vector for circMet silencing was designed based on pAAV-CMV-Flex-MIR30shRNA-EGFP vector and packaged by Obio Technology (Titer: 1×10^{13} vg/m, Shanghai, China). Cdh5-Cre mice (6-8 weeks old) were anesthetized by the intraperitoneal injection of ketamine (80 mg/kg) and xylazine (4 mg/kg). The pupils were dilated by the administration of 0.5% tropicamide. The 33-gauge sharp needle was used to make a scleral puncture at 0.5 mm posterior to the limbus. Approximately 1.0 μL of Cre-dependent circMet shRNA virus was subsequently injected into the vitreous cavity to ensure the specific inhibition of circMet expression in endothelial cells. Cdh5-Cre mice without Cre-dependent circMet shRNA injection were used as the control group.